Combined Optical and Radio-Frequency Measurements of a Lightning Megaflash by the FORTE Satellite

Michael Peterson[1], Tracy E. L. Light[1], Xuan-Min Shao[1]

[1]ISR-2, Los Alamos National Laboratory, Los Alamos, New Mexico

Corresponding author: Michael Peterson (mpeterson@lanl.gov), B241, P.O. Box 1663 Los Alamos, NM, 87545

Key Points:

- Combined FORTE optical / RF instrumentation document the evolution of a mesoscale oceanic lightning "megaflash"
- Optical observations reveal the development of long horizontal lightning channels that extended over 82 km
- RF observations indicate substantial leader activity accompanying channel development as well as 4 distinct +CG strokes spread throughout the flash area

LA-UR-20-30147

Abstract

The optical and VHF instrumentation on the FORTE satellite is used to document the combined phenomenology evolution of a lightning "megaflash" – mesoscale lightning that propagates laterally over exceptional distances. We identify a FORTE flash whose maximum extent was 82 km and inferred length over multiple distinct branches exceeded 100 km. This flash lasted 1.2 s and produced 250 optical and 591 RF events. We find that the channel development mapped by FORTE's pixelated lightning imager (LLS) occurred at a typical speed of 2.6×10^5 m s^{-1} and was accompanied by sustained periods VHF emission that could individually exceed 100 ms in duration. The impulsive IC events generated by the flash indicate that this development occurred at altitudes between 3 and 8 km. Four +CG strokes were identified in the VHF waveform data that are responsible for two of the three highly-radiant LLS groups (the third radiant group came from a possible -CG while 2 of the +CGs were not as optically bright as the others). These strokes occurred at different locations throughout the flash footprint with the most distant strokes separated by approximately 50 km. These space-based observations match previous observations of megaflashes from space as well as ground-based measurements of slow negative leader development during "spider" lightning, suggesting that FORTE is sensing the same phenomena.

Plain Language Summary

Pixelated lightning imagers map the lateral development of lightning flashes by recording how the locations of radiant pulses produced by lightning change over time. Most lightning flashes measured by instruments including NASA's Lightning Imaging Sensor (LIS) and NOAA's Geostationary Lightning Mapper (GLM) are small and repeatedly illuminate the same cloud region with little apparent motion between pulses. However, certain thunderstorms are able to produce "megaflashes" that start in one place and then develop up to hundreds of kilometers horizontally from the initiation point. These propagating flashes pose a unique hazard because they can strike the ground in places where lightning is not expected.

We use measurements from the FORTE satellite to investigate what radio-frequency signals accompany the optical signatures of a lightning megaflash. RF data provide insights into the physical origin of the optical lightning emissions. A detailed analysis of a megaflash 82 km across reveals that optical flash propagation is accompanied by abundant VHF signatures of leader development as well as multiple distinct +CG strokes at different places across the flash.

1 Introduction

Lightning generates optical signals by rapidly heating the air surrounding the lightning channel. Temperatures along the channel may exceed 20,000 K (Prueitt, 1963), causing ionization of the major atmospheric constituent gasses. The ionization, excitation, and recombination of atmospheric constituents results in particularly strong optical emissions in the near-infrared neutral oxygen and neutral nitrogen atomic lines. Optical pulses are produced by Cloud-to-Ground (CG) strokes as well as a myriad of in-cloud processes that illuminate the lightning channel.

Space-based lightning imagers such as NOAA's Geostationary Lightning Mapper (GLM: Goodman et al., 2013) and NASA's Optical Transient Detector (OTD: Christian et al., 2003) and Lightning Imaging Sensor (LIS: Christian et al., 2000; Blakeslee et al., 2014) report the spatial and temporal evolution of individual flashes by measuring transient changes in cloud-top illumination from the lightning discharges that comprise the flash. OTD, LIS and GLM record the optical radiance in a narrow band centered on the neutral Oxygen line triplet at 777.4 nm to take advantage of the emissions peak resulting from these underlying physical processes (Christian et al., 2000; Goodman et al., 2010).

Optically bright lightning processes vary in terms of extent, speed, current, and polarity. Identifying reliable optical signatures for specific processes such as strokes (Koshak, 2010) has proven difficult because optical measurements provide little information on the nature of the source beyond the intense heating along the channel, and also because the optical signals recorded from space have been modified by scattering and absorption in the cloud medium (Thomson and Krider, 1982; Koshak et al., 1994; Light et al., 2001a,b; Thomas et al., 2000; Suszcynsky et al., 2000). Scattering causes the optical signals to be diluted in space and

broadened in time. Flashes that occur in particularly inhomogeneous clouds have their footprints sculpted by spatial distribution of hydrometeors in the thundercloud (Peterson et al., 2017a). Flashes that occur near a cloud boundary often take on an irregular shape as the radiance measured from space follows the boundary (Peterson et al., 2017b), while dense convective cells can produce "holes" in otherwise contiguous flash footprints by blocking light from reaching orbit in sufficient quantities to trigger the instrument. Radiance can also reflect off the sides of neighboring clouds or the tops of lower cloud decks to expand the flash footprint far beyond the extent of the parent thunderstorm (i.e., Figure 1 in Peterson and Liu, 2013). Due to these scattering effects, the optical signals recorded by OTD, LIS and GLM may contain as much information about the cloud scene as they do about lightning.

Still, there are optical signatures in the lightning imager data that reveal key aspects of the physical evolution of the lightning flash. Lateral propagation in the optical flash structure, for example, indicates horizontal leader development (Peterson et al., 2018). LIS and GLM observe both the flickering at the ends of developing lightning channels and the waves of radiant energy retracing an established channel back to its origin that have been noted in ground-based observations (Mazur et al., 1998; Winn et al., 2011). The optical pulses that map the development of these flashes are small and relatively dim, so the shapes of their footprints (as imaged by a lightning imager with kilometer-scale pixels) are not modified substantially by scattering. Thus, the structure of propagating optical flashes measured by space-based lightning imagers approximates a two-dimensional vertically-integrated view of the three-dimensional flash structure that would be mapped by a Lightning Mapping Array (LMA: Rison et al., 1999). The two key caveats with optical space-based lightning mapping are the large pixel footprints (4-5 km for LIS and 8-14 km for GLM) and the decreasing source detection efficiency as the optical

thickness of the intervening cloud layer increases. Leader propagation through deep convection that is routinely observed by LMAs (i.e., Lang et al., 2017) is generally not resolved from space. As a result, the LIS / GLM measurements of flash extent are a minimum estimate for the scale of lightning that mostly captures long horizontal channels in stratiform and anvil clouds (Peterson and Liu, 2011).

We have used lightning imager data to measure the horizontal extent of propagating flashes and to calculate their development speeds (Peterson et al., 2018). We have also defined "series" features (Peterson et al., 2017b) to describe distinct periods of sustained optical emission that typically accompany widespread branching and recoil waves, but can also capture lightning emissions related to gigantic jets (Boggs et al., 2019) and return stroke continuing currents (Bitzer, 2017). Peak optical emissions during individual series are also used to define an optical multiplicity that describes how often flashes light up well above the numerous low-radiance pulses associated with cloud discharges (Peterson and Rudlosky, 2019). The optical multiplicity is advanced by strokes as well as K-changes that both produce strong emission along the channel.

While these optical-only capabilities are useful for analyzing lightning activity, a comprehensive view of lightning physics is achieved when optical and RF measurements are combined to describe the same flash. We previously used coincident optical and VHF measurements taken by the Fast On-Orbit Recording of Transient Events (FORTE) satellite to identify the physical processes responsible for the optical signals recorded by its pixelated lightning imager during a hybrid CG flash (Peterson et al., 2020a). In this study, we use the same approach to investigate the combined-phenomenology evolution of a horizontally-expansive lightning megaflash observed over the open ocean near the Canary Islands.

2 Data and Methodology

The FORTE satellite was a unique platform for examining lightning from space because it contained both optical and RF payloads for observing transient lightning pulses, and because its instrumentation was operated in campaign mode. The optical / RF trigger settings, data record lengths, and RF frequency bands were periodically reconfigured on-orbit over the FORTE mission. FORTE thus provinces multiple different types of coincident data that can be used to assess various aspects of lightning discharges. A detailed description of the FORTE RF payloads is provided in Jacobson et al. (1999), while the optical payloads are described in Suszcynsky et al. (2000, 2001). Moreover, the FORTE mission and its key scientific findings are reviewed in Light (2020). The sections below summarize the RF and optical payload configurations that pertain to our megaflash case of interest.

2.1 The FORTE Optical Lightning System

The optical payload on FORTE was known as the Optical Lightning System (OLS). The OLS consisted of two different optical instruments. A high-speed photodiode detector recorded broadband (0.4 μm – 1.1 μm) lightning pulses in 2 – 6 ms records with a 15 μs sampling interval. The PDD could be triggered by optical lightning pulses anywhere within its 80° field of view. If we think of the PDD as a single-pixel lightning imager, then it would have an effective frame rate of 66,667 FPS. In both Peterson et al. (2020a) and this study, the PDD was configured to trigger autonomously and produce 1.92 ms records of optical lightning activity. The PDD had a dead time between records that was approximately equal to the record length. Thus, we will see ~2 ms gaps between the PDD records from successive triggers during periods of sustained

optical emission. We also noted in Peterson et al. (2020a) that the PDD stops reporting after a specific number of triggers on flash time scales. As the megaflash case occurred around the same time as the previous hybrid CG flash case, this 20-trigger maximum will be a limitation in the present study as well.

The second OLS instrument was a pixelated lightning imager known as the Lightning Locating System (LLS). The LLS consisted of the same front-end optical assembly and fixed-position CCD focal plane assembly used by LIS that was provided by NASA Marshall Space Flight Center, and an operations and signal processing module designed by Sandia National Laboratories. The LLS was designed to have a lower (405 FPS) frame rate than LIS (500 FPS). The key role of the LLS was to geolocate lightning sources. Coordinated observations with the PDD would then enable light curves to be resolved at orders of magnitude finer time scales than LLS or LIS could measure.

Because the LLS signal processing module was designed by Sandia, the artifact filters and cluster feature algorithm developed for LIS (Christian et al., 2000) were not applied to the LLS data during the FORTE mission. LLS observations in its standard operating mode include only pixel-level "event" detections. Events are recorded whenever the measured radiance in a given CCD pixel during a single 2.47-ms integration frame exceeds a noise-riding threshold above the radiance of the background scene. Note that this description of events follows the NASA terminology. The raw LLS events (subsequently termed "super-events" because they are conceptually similar to the proposed concept of "supergroups" in Tillier et al., 2019) can describe the same pixel being illuminated for multiple frames. For consistency with the other sensors such as LIS, we extract the single-frame pixel detections from the raw LLS super-events and use the standard term "events" to describe them. Artifacts are handled by simply ignoring

subsequent detections from the same pixel once events are recorded in that pixel during two adjacent integration frames. This filter prevents the LLS from measuring sustained optical emission from a stationary source (i.e., continuing current with a return stroke), but still permits the LLS to record sustained emission from propagating sources (i.e., lateral flash development, K-waves).

2.2 The FORTE Radio Frequency (RF) System

The Radio Frequency (RF) system was comprised of three broadband receivers connected to the two identical Log-Periodic Antennas (LPAs) mounted along FORTE's 10-m nadir-pointing boom. The three receivers were divided between two RF payloads known as TATR and HUMR. TATR consisted of 2 independent RF receivers (TATR/A and TATR/B) that could each be tuned to measure one of the FORTE antennas over a 22-MHz subband. The record lengths and the ratio of pretrigger to posttrigger data could also be configured. HUMR, meanwhile, sampled a wider (85 MHz) band over longer records that typically lasted 3 ms.

This study and Peterson et al. (2020a) both use TATR observations from late 1999 when it was configured to record lowband (26 – 48 MHz) waveforms and set to trigger autonomously. In its autonomous mode, TATR monitored the RF power in eight RF channels that were each 1-MHz wide. Whenever the received power exceeded the noise-riding background value in one of these channels by a certain threshold, the instrument would report an alarm. Triggers require multiple simultaneous alarms in the 8 channels, and the number of alarms required to trigger the instrument and report an event was a commandable parameter. Typically, only RF events that triggered 5 of the 8 channels are examined (i.e., Jacobson et al., 2000), but we instead consider

all TATR triggers during a time window encompassing LLS flashes (+/- 330 ms) in order to capture the weakest lightning phenomena detectable from orbit.

While optical lightning signals are modified by scattering in the cloud, VHF pulses are modified by the ionospheric plasma between the source and satellite. Ionospheric dispersion causes a frequency-dependent group delay in the recorded VHF pulses. Signals on the low-frequency side of the band arrive after the high-frequency signals, and the waveforms appear "chirped" (Jacobson et al., 2000). The severity of the dispersion depends on the Total Electron Content (TEC) of the ionospheric slant path between the source and sensor. By fitting the dispersion in the received signal to a physics-based mathematical model, we can "dechirp" the data and align the VHF waveforms to their vacuum time of arrival. The dechirping process also yields an estimate for the ionospheric TEC encountered by the signals along their slant path through the ionosphere, which we can further use to identify signals that come from elsewhere in the FORTE field of view (Jacobson et al., 1999.

Unlike in the hybrid CG case in Peterson et al. (2020a), we find no evidence that thunderstorms located at different slant angles are contributing TATR triggers during the duration of the megaflash considered here. However, there is one TATR trigger in the flash that resulted from an on-board discharge. This trigger was a single impulsive event that produced the strongest peak RF power over the flash duration, but had no evidence of ionospheric dispersion in the event waveform data. This on-board discharge event is preserved in the RF waveform records to show how these features contaminate natural lightning signals, but it is otherwise ignored in the broader discussion of the flash.

2.3 FORTE combined-phenomenology lightning cluster data

Though flash cluster data was not created from the LLS events during the FORTE mission, the LIS (Christian et al., 2000) and GLM (Goodman et al., 2010) flash cluster algorithms have been documented in the literature and can be adapted for use with FORTE. We used the GLM algorithm as the basis for constructing a combined-phenomenology lightning cluster feature dataset in Peterson et al. (2020a) that includes both optical and RF features.

Design considerations for the full FORTE cluster feature dataset are described at length in Peterson et al. (2020a) and we will discuss only the optimal data structure for FORTE analyses here (shaded boxes in Table 1 from Peterson et al., 2020a). LLS events are used to define "group" features that represent contiguous regions on the LLS CCD array that are lit up during the same 2.47-ms integration frame. Groups are then clustered into LLS "flashes" using the same Weighted Euclidian Distance (WED) model as LIS / GLM. The distance and time thresholds for assigning two groups to the same flash are 16.5 km and 330 ms, respectively. If a new group occurs that could belong to multiple flashes, a "full fit" matching technique is employed that merges the two candidate flashes into a single flash cluster. "Series" features are also constructed that describe sustained optical emission within individual flashes. Series encompass all groups in a given flash that occur either sequentially or following a 1-frame gap. Finally, thunderstorm areas of interest (or "areas") are constructed by applying the WED model to the flash cluster data with the same 16.5 km distance threshold and no time threshold (though all flashes in the same area should occur during the same FORTE orbit).

The FORTE PDD and RF data are ingested into the LLS hierarchy at the event level after making a minor change to the "event" definition. In the LIS / GLM literature, an event is defined as a single triggered pixel on the CCD array during an integration frame. We slightly generalize this definition to describe an event as a unique trigger during the millisecond-scale triggering

interval associated with the instrument. The PDD and RF system can have only one unique trigger from their FOVs at a given instant, while the LLS would have a unique trigger for each pixel that lights up in a given frame. With this change, we can construct lightning cluster feature data structures (i.e., areas, flashes, groups) for the PDD and RF system that parallel the LLS hierarchy. The high sampling rates of these instruments also allow us to extend the data tree to finer time scales that occur within a single "event." We define "pulses" as features describing periods of sustained emission above a noise-riding background threshold that occur within a single event record. We also define "samples" as single calibrated measurements at the native sampling rate of the instrument. Events are the parents of pulses and the grandparents of samples. We finally integrate the LLS, PDD, and RF features by defining "step-parent" relationships that assign PDD and RF events, pulses, and samples to LLS groups, series, flashes, and areas.

3 Results

The present study aims to investigate the RF signatures that accompany lateral propagation in the optical lightning imager data. In particular, we will be focusing on the large-scale propagation that we see with megaflashes where the lateral development is widespread and organized along multiple distinct branches. LMA networks have mapped extensive propagating flashes that measure 321 km from one end to the other (Lang et al., 2017), while GLM has recorded cases that exceed 500 km in length (Peterson, 2019c; Lyons et al., 2019). The most exceptional megaflash cases recognized as lightning extremes by the World Meteorological

Organization (WMO) are now two different cases of GLM flashes that reached 709 km in extent and 16.73 s in duration, respectively (Peterson et al., 2020b).

The common aspect shared by all of these exceptional megaflash cases is that they primarily develop through the electrified stratiform region of a large (mesoscale) mature or dissipating storm system. Stratiform clouds become electrified through a combination of the advection of charged ice particles from the convective core (Carey et al., 2005) and in-situ charging in the radar bright band (Rutledge and MacGorman, 1988) that may be enhanced by local mesoscale updrafts (Ely et al., 2008; Lang and Rutledge, 2008). These processes generate multiple vertically-thin charge layers that can extend laterally over hundreds of kilometers (Marshall and Rust, 1993; Stolzenburg et al., 1994; Lang et al., 2004; Marshall et al., 2009) and act a conduit for lightning propagation.

The combined optical and RF phenomenology of complex horizontally-propagating "spider" lightning was studied from the ground in Mazur et al. (1998) using a whole sky intensified camera system co-located with a VHF interferometer. They concluded that spider lightning consists of slow (2-4 x 10^5 m s^{-1}) negative leaders that produce transient optical pulses at the tips of the branching channels and occasional continuous illumination along the entire channel resulting from sustained current flow that may last tens to hundreds of milliseconds. Because the development speeds, VHF signatures, and flickering at the ends of branches in the optical measurements are all similar to stepped-leaders in negative CG flashes, they suggested that spider lightning results from the same underlying physical processes.

The FORTE satellite is equipped to make similar optical and VHF measurements of horizontally-propagating lightning to Mazur et al. (1998) from space. FORTE observations have

an expanded horizontal domain compared to the range from a single site to the local horizon, and its orbital measurements are mapped in geographic coordinates rather than spherical coordinates surrounding the site. Thus, we do not have to assume an altitude for the lightning channels to compute lateral distance or propagation speed. However, the key limitation to observing megaflashes with FORTE is the short view times over a given thunderstorm (on the order of minutes) due to its low Earth orbit. The FORTE satellite would have to be in the right place at the right time to see a megaflash – and this is why megaflashes are rarely observed in the OTD / LIS records. The FORTE LLS has detected a small number of megaflashes whose extents are < 100 km, but whose total lengths are considerably larger. In the following sections, we will examine the longest of these LLS megaflash cases in detail.

3.1 Overview of FORTE measurements during an oceanic megaflash on 12/3/1999

Megaflash cases are identified in the FORTE record according to the maximum great circle distance between LLS groups. This is a low estimate of flash scale because megaflashes do not propagate directly from one end to the other, but instead take a meandering path through the electrified cloud. Peterson et al. (2018) attempted to measure total flash length by constructing skeleton images of the two-dimensional flash structure reported by LIS and found that flash length was usually 2-3 times greater than its reported extent.

The top LLS flash in terms of extent occurred over the Atlantic Ocean between the Canary Islands and the Azores on 12/3/1999 at 22:30:22 UTC (23:30:22 local time in Santa Cruz de Tenerife). It was 82 km across and produced 69 LLS series, 98 LLS groups, and 230 LLS events over a duration of 1180 ms. In total, it illuminated a cloud-top area of 5203 km^2 with the

largest group in the flash illuminating 2386 km^2 of cloud. In addition to these LLS triggers, the PDD contributed 20 optical events and TATR recorded 591 VHF events.

The LLS Flash Extent Density (FED: Lojou and Cummins, 2004) plotted in Figure 1a indicates that the flash rate for the storm was low (3 flashes in 15 minutes), and that there were no intense thunderstorms nearby that could have contributed the large number of TATR triggers during the flash duration. The trigger rates in Figure 1b show that there was only 1 isolated optical trigger in the minute leading up to the flash and that subsequent triggers after the flash occurred more than 1 s following the final LLS group. Unlike the hybrid CG case in Peterson et al. (2020a), this case did not contain any RF triggers before first LLS light or after final light.

3.2 Evolution of optical signals from the megaflash

Figure 2 documents the overall evolution of the LLS flash. The central panel (Figure 2c) shows the plan view of the events and groups in the flash. Normalized event energies from each pixel on the CCD array are summed to produce a color contour plot representing the spatial radiance distribution. The progression of groups is traced in time with line segments that connect each group centroid to its nearest preceding group. The greyscale color palette denotes the sequential group index from dark (first group) to light (final group), and is standardized between all panels in Figure 2. Figure 2a shows the longitudinal extent of all groups in the flash while Figure 2d shows their latitudinal extents. Figure 2b displays a histogram of group energy presented as a sigma level (the number of standard deviations above or below the mean for all groups in the flash). Figure 2e and f, finally, show timeseries of group area and normalized group energy.

The flash began along the southwestern flank of its footprint (Figure 2c) and propagated to the northeast. At least 6 primary branches spanning more than 20-km (~2 pixels) can be noted in the group-level structure that contain smaller features propagating laterally off the main channels. The LLS groups associated with this lateral development are typically dim and small (100 – 200 km^2 in Figure 2e) – yet they account for the clear majority of optical triggers from the flash. Only 3 groups reach the +1-sigma level (Figure 2b). We use the 1-sigma group count to define an optical multiplicity parameter that quantifies how often a given flash lights up beyond the baseline radiance from these common dim cloud pulses under the specific viewing conditions of the flash. The optical multiplicity for this flash would thus be 3, with intervals of 43 ms and 311 ms separating the series containing these bright groups. The FORTE megaflash considered in this study produced groups that reached an exceptional 8-sigma above the average group energy for the flash.

3.3 Combined optical and RF assessment of flash evolution

The timeseries in Figure 3 show the combined-phenomenology evolution of the LLS flash. Optical group energies are plotted in Figure 3a for LLS and Figure 3b for PDD and are normalized to the peak received group energy for each instrument on a logarithmic scale. TATR event records are dechirped and "prewhitened" (to remove narrowband carrier waves), and then the band-averaged peak VHF power for each trigger is shown in Figure 3c. Like the optical energy, RF power is normalized relative to the strongest emissions during the flash window. The TATR pulses recorded in each event are categorized as isolated impulses (single pulse), isolated pulse pairs (single pair of pulses representing an IC source with a ground reflection), pulse trains (multiple pulse pairs per TATR record), or diffuse / mixed pulses (broad pulses that may include superimposed impulsive features). TATR records that do not contain any classifiable pulses are

designated “sustained featureless emission.” We divide the flash duration into 2-ms bins (comparable in scale to PDD records or LIS / GLM groups) and then compute the fractions of each pulse type per bin in Figure 3d.

Because we know the geographic position of the flash from the LLS observations, we can compute the altitude of impulsive IC sources using the satellite position and the time delay between pulses in each Trans-Ionospheric Pulse Pair (TIPP: Holden et al., 1995). Estimated altitudes for the isolated impulsive IC events and pulse trains from Figure 3d are shown in Figure 3e. Finally, Figure 3f integrates the received optical LLS energy and TATR antenna response (in $V^2\ m^{-2}$) to compare the accumulation of optical / RF signals over the duration of the flash.

In our previous -CG case (Peterson et al., 2020a), the TATR triggers were intermittent and dominated by impulsive IC events and K-changes. Leader activity ahead of the return stroke produced sustained featureless emission that strengthened over multiple TATR records as the stepped leader developed towards the surface and then a single strong VHF pulse occurred upon seawater attachment. The TATR records in the current megaflash case, by contrast, are dominated by periods of sustained featureless VHF emission over tens to hundreds of milliseconds (Figure 3d). The longest-lasting TATR series feature started 200 ms into the LLS flash and then persisted for 169 ms. Of the total 591 TATR events, 516 were classified as sustained featureless emission. The remaining 75 TATR records contained 38 TIPPs, 38 diffuse pulses, and 5 isolated single impulses (including one from the on-board discharge mentioned previously). Note that the total number of pulses is greater than the number of events due to certain events containing multiple pulses.

As with the energy budget from previous -CG flash in Peterson et al. (2020a), optical energy from the megaflash accumulated rapidly in 1-2 frame increments in Figure 3f, while the RF signals accumulated gradually over longer time intervals. The three high-radiance groups in the LLS flash that exceeded the 1-sigma level contributed 5%, 30%, and 17% of the total energy of the flash (total: 52%). The remaining 95 groups contributed 48% of the total energy.

While most TATR waveform records appear to originate from IC sources, four TATR events contained the signatures of positive-polarity CG strokes described in Light et al. (2001b). A spectrogram for the first of these strokes (at 14 ms into the LLS flash) is shown in Figure 4. +CG events have a quick onset typically followed by a broad VHF pulse due to considerable in-cloud activity following attachment. This lingering tail can last for tens of milliseconds, spanning multiple TATR records. Mazur et al. (1998) noted comparable behavior from the ground in their analysis of +CGs in spider lightning.

The other +CGs in the FORTE megaflash occur at 282 ms, 335 ms, and 592 ms into the LLS flash with similar TATR records to the spectrogram shown in Figure 4. The key difference with these later +CGs is that they occurred under a stronger RF background from the widespread leader activity in the later stages of the flash. We use these RF signatures to divide the flash into 4 phases: initial horizontal development of the lightning channel and first +CG stroke (0 ms to 265 ms), peak optical emission during the second +CG stroke followed by weaker emission during the third +CG (265 ms to 400 ms), further branching along the northern flash extent leading up to the fourth +CG stroke (400 ms to 700 ms), and then final optical activity after the continuous VHF emission ceased (700 ms to 1180 ms). The evolution of the flash during these phases is discussed below.

4 Discussion

4.1 Initial horizontal development of the lightning channel and first +CG stroke

An evolution plot for the first optical / RF events in the flash is shown in Figure 5. The key difference between the format of Figure 3 and Figure 5 is that the group area timeseries is removed and a TATR RF power timeseries is displayed in its place. PDD sample energies are also plotted in blue alongside the normalized LLS group energies in Figure 5e. The LLS flash began with a single-pixel event at t = 0 ms that has slightly less than 1% of the optical energy of the most radiant group in the flash. The baseline for single-pixel detections is ~0.7% to 1% of peak emission. These optical emissions from individual LLS pixels were too faint / localized for the PDD to trigger.

The first 2 TATR events were recorded 4 ms and 14 ms into the LLS flash. The first TATR event consisted of an impulsive IC TIPP with additional IC pulse pairs embedded in the VHF background. Unlike Peterson et al. (2020a), this flash did not start with a powerful TIPP waveform from a Narrow Bipolar Event (NBE). Any IC events that could have occurred before first LLS light were too weak to trigger TATR.

The first +CG stroke occurred 14 ms after the first LLS event and 10 ms after the first TATR event. The first long period of continuous RF triggering occurred following this stroke (Figure 5f). During this time, two impulsive IC events were noted at ~5 km altitude as well as an isolated single impulse. This single-peak event at 22 ms was caused by the on-board discharge noted previously. The remaining TATR triggers from 14 ms to 41 ms were all diffuse featureless

emission associated with leader activity. The PDD triggered continuously over this period, demonstrating that there was sustained optical emission accompanying the continuous VHF activity. The LLS only triggered twice, however, with a 5-pixel group at 14 ms and a single-pixel group at 24 ms. The optical energies in all lit-up pixels were near the minimum for the flash (Figure 5c), suggesting that the emissions that triggered the PDD were spread over a large area with energy densities only occasionally exceeding the LLS detection threshold in its individual pixels.

The continuous TATR triggering stops at 41 ms and then there is a lull with only 2 TATR triggers (one IC pulse train at 4.2 km altitude and one sustained featureless emission) until 112 ms into the LLS flash. The time period from 112 ms until 215 ms depicted in Figure 6 describes the incremental development of the flash to the north and east through small / dim groups illuminating the tips of the extending branches. RF activity is intermittent before 200 ms and evenly distributed between IC pulse pairs / trains from sources at 6 km altitude and sustained featureless emission. The LLS and PDD trigger simultaneously at 157 – 160 ms following a pulse train with a relatively weak peak RF power, and the PDD continues to trigger until its 20 triggers are exhausted by 210 ms.

TATR began its longest period of continuous triggering at 200 ms. Unlike the previous continuous period, it did not begin with a stroke. The PDD recorded sustained emissions starting at 160 ms. The remainder of the initial IC lateral development phase from 230 ms until 265 ms is shown in Figure 7. The first LLS groups at 235 ms resulted from the tips of all existing channels being simultaneously illuminated. Then the first 1-sigma bright group is detected during the next integration frame (starting at 238 ms) where nearly the entire extent of the main channel lit up at once. VHF waveform analysis of what caused this behavior is inconclusive, as the high VHF

433 background obscures portions of the waveforms that are important for pulse characterization.
434 Figure 3d shows that sustained featureless VHF emission accompanied the first 1-sigma LLS
435 group. However, a detailed analysis of the TATR waveforms found a single narrow peak in the
436 TATR trigger at 235 ms consistent with a -CG. This peak is so poorly resolved that the
437 automated dechirp algorithm fails to find it - causing no TEC estimate to be retuned and the
438 event to be labeled as sustained featureless emission.

439 We do not see the increasing VHF emission leading up to attachment that typically
440 accompanies -CGs in the event recorded at 235 ms, as it would be buried in the high VHF
441 background. Furthermore, the peak occurred at the end of the TATR record due to the
442 continuous TATR triggering. Thus, we cannot be certain that this was a single solitary peak from
443 a -CG. An alternate explanation could be that it was an impulsive IC event where the second
444 peak in the TIPP occurred during the dead time between TATR records. Of these two
445 possibilities, the strong optical emission accompanying the event suggests that the -CG
446 explanation is more likely - but this is not assured.

447 The subsequent groups over the next 20 ms were all located along the main channel and
448 constituted one of the longest-lasting LLS series features in the flash (15 ms in duration). These
449 factors seem to indicate a sustained flow of current down the channel that is only partially
450 resolved in the pixelated LLS data. PDD data would be required to confirm continuous optical
451 emission (as with the first +CG). The maximum group separation by 260 ms was 68 km, and this
452 lateral development allows us to infer an average propagation speed 2.6×10^5 m s^{-1}.

453 The development of this FORTE flash is consistent with the ground-based observations
454 of spider lightning from Mazur et al. (1998). We find pulses illuminating the tips of branched

channels in the flash and luminosity along the channel that may have been sustained for many milliseconds in agreement with their video observations. The lateral development speed of our flash also fits within their 2-4x10^5 m s^{-1} range for the slow negative leaders that occur in spider lightning events, while the sustained RF emission recorded by TATR also agrees with their RF records of strong continuous VHF radiation from the slow leader (Figure 12 and 13 in Mazur et al., 1998). Unlike the previous ground-based results, the FORTE LLS did not map lightning activity that was distinct from the propagating spider event. If additional fast negative leaders or positive leaders occurred in other parts of the lightning "tree" as described in Mazur et al. (1998), they were either too weak to be resolved from space or co-located with the geographic extent of the developing spider flash.

4.2 Optical emission during second and third +CG strokes

The most radiant group in the flash (8-sigma) occurred at 282 ms in the evolution plot in Figure 8. This was the second bright group (> 1-sigma) in the flash, with the first describing the illumination of the long horizontal channel during a possible -CG. The RF power coincident with this second bright group increased rapidly by 10 dB and then fell back to the average sustained RF power level over a period of 12 ms – conforming to the +CG signature that we saw with the first stroke in Figures 4 and 5. The long-duration VHF activity following the stroke (also seen in the +CG strokes in Mazur et al., 2008) is interesting because it was not noted in the TATR waveforms from Light et al. (2001b), where the "normal" (i.e., non-megaflash) +CG pulses were shown to last between ~150 μs and 500 μs.

This behavior may be a unique feature of VHF emission from megaflashes that can access charge from throughout their vast networks of ionized lightning channels during strokes

and funnel it to the surface. We see evidence for this in the LLS data from this second +CG. This second +CG stroke was located along the northeastern flank of the flash. If we assume that the strokes are co-located with the centroid of the brightest simultaneous LLS groups, then the first and second +CG strokes were separated by approximately 50 km. However, the 8-sigma bright group is not the only LLS activity during the second +CG. Two single-pixel groups occurred during the VHF tail that appear to extend the existing channel: one at the flash origin, and one on the eastern flank of the flash south of the second +CG (though, still within the cloud-region that the stroke illuminated two frames prior). This indicates that the whole 60-km channel was active during this stroke, with these new breakdowns contributing to the VHF tail. It is likely that the channel was continuously illuminated (as we saw with the PDD waveforms during the first stroke), but that LLS only triggered intermittently in the pixels corresponding to emissions with high energy densities. However, this is only speculation as the PDD triggers that could confirm sustained optical emission had been exhausted by this point in the flash.

The second of the single groups in Figure 8 would become important because it marked the initial development of a new branch in the flash that would go on to produce the third +CG stroke at 337 ms. Flash evolution at the time of the third stroke is shown in Figure 9. While this stroke was not accompanied by strong VHF emission (only 5 dB above the baseline RF power during the flash), it was optically bright – producing a LLS group with more than 10% of the energy of the 8-sigma stroke. It likewise has a long VHF tail (12-15 ms following the primary pulse) within which LLS activity could be noted back at the flash origin – again, suggesting that the whole channel was active during this period. The single-event group at 362 ms marks the last time when LLS detected activity near the flash origin until the final phase of the flash.

4.3 Channel extension and branching leading up to the fourth +CG stroke

The period following the third +CG strokes is marked by continued incremental lateral development of the existing branches along the lightning channel and the later establishment of a new northwestern major branch. The first portion of this period from 450 ms to 550 ms is plotted in Figure 10, and it lacked the sustained VHF emission that we noted previously with the initial development of the flash. The impulsive IC events during this period originated from a broad range of altitudes between 4 km and 7 km. TATR events included isolated IC pulse pairs, sustained featureless emission, and diffuse RF pulses as the northeastern and eastern branches were extended by 1-2 pixel LLS groups illuminating their tips. Small features can also be noted on the order of 1 pixel or less departing from the main channel (light grey features in Figure 10c). These smaller features may be short branches or they might be caused by uncertainties in the source locations due to the pixelated LLS grid.

The final group during this period established the beginning of a new northern branch that would continue to develop to the northwest over the next few groups and go on to produce the fourth +CG stroke. The initial development of the northwestern branch from 540 ms to 590 ms is shown in Figure 11. There are a few RF-only triggers from 540 ms to 550 ms in Figure 11e,f followed by sustained RF activity that resembles the initial TATR triggers in the flash. However, the strong RF pulse at the beginning of the sustained RF triggering appears to be a K-change rather than a stroke in this case due to its relatively-slow rise time. This sustained VHF emission lasted ~70 ms and appears to describe leader activity along only the northern branches of the flash (Figure 11c).

The time period from 585 ms to 700 ms is shown in Figure 12 and includes the fourth +CG stroke at 593 ms. The VHF pulse reached 12 dB above the RF background and generated the second-most radiant optical group in the LLS flash at 4-sigma. The LLS group had an oblong

footprint with the most radiant pixels following the linear path of the northwestern branch (Figure 12c). As with the previous +CG events, a VHF tail can be noted lasting for 20 ms following the stroke. Subsequent groups in Figure 12 describe re-illumination along the northeastern branch of the flash and further extension of some of the smaller branches away from the main channel.

4.4 Final development after continuous RF emission ceased

The last 480 ms of the flash is shown in the evolution plot in Figure 13. The sustained featureless VHF emission that accompanied the slow leader ceased by 670 ms, and this final period was marked by intermittent impulsive IC events and diffuse K-changes. All but one of the LLS groups occurred along the northeastern branches in the flash. The group at 722 ms is the exception, as it illuminated part of the initial southwestern branch. The group at 752 ms extends the flash to its maximum lateral extent of 82 km across. The final impulsive IC event near 8 km altitude occurred at 820 ms, while the four last impulsive IC events in the flash were located at or below 6 km altitude. The final RF event was a diffuse pulse that had optical coincidence at 1120 ms, while the final LLS group was a single-event trigger that occurred 60 ms later along the northernmost extent of the flash structure.

5 Conclusion

We use coincident optical and RF instrumentation aboard the FORTE satellite to examine the combined-phenomenology evolution of an oceanic megaflash that was 82 km across and lasted nearly 1.2 s. There are a number of distinct features in the optical / RF signatures that stand out in this flash, which may be unique to this distinct class of lightning.

No RF triggers occurred before the first optical event, while the initial RF / optical signals were some of the weakest recorded from the flash. The 591 TATR events produced by this megaflash were dominated by sustained featureless VHF emission that constantly triggered TATR over periods lasting tens to hundreds of milliseconds. Impulsive IC events occurred at altitudes between 3 and 8 km. The LLS groups describe the incremental lateral development of the lightning channel at a typical development speed of 2.6×10^5 m s^{-1}. Three of these groups were particularly radiant and accounted for 5%, 38%, and 17% of the total optical energy from the flash (52% from all three, combined). The top two most radiant groups come from +CG strokes, while the third appears to have resulted from a -CG stroke, though RF waveform analysis was inconclusive. Two additional +CG strokes were also identified whose optical energies did not reach the 1-sigma level for the flash.

These observations are consistent with previous ground-based studies that show "spider lightning" in horizontally-propagating flashes occurring as slow negative leaders ($2\text{-}4 \times 10^5$ m s^{-1}) that develop at low levels (~4 km) in mature / dissipating stratiform clouds via the same apparent mechanism as the stepped leaders that precede negative return strokes. Similarities in the general optical / RF phenomenologies and the signatures that are present suggest that we are sensing the same processes from orbit that they recorded at ground level. The sustained RF emission during extensive flash propagation in the optical data confirm that this behavior is related to leader activity in the cloud and provides additional context for our previous assessment of the speed and scale of optical flash development (Peterson et al., 2018).

Acknowledgments

Los Alamos National Laboratory is operated by Triad National Security, LLC, under contract number 89233218CNA000001. The data presented in this study are located at Peterson (2020).

References

Bitzer, P. M., 2017: Global distribution and properties of continuing current in lightning, *J. Geophys. Res. Atmos.*, **122**, 1033–1041, doi:10.1002/2016JD025532

Blakeslee, R. J., H. J. Christian, M.F. Stewart, D.M. Mach, M. Bateman, T.D. Walker, D. Buechler, W.J. Koshak, S. O'Brien, T. Wilson, E.C. Colley, T. Abbott, J. Carter S. Pavelitz, C. Coker, 2014: Lightning Imaging Sensor (LIS) for the International Space Station (ICC): Mission description and science goals, *XV Int. Conf. Atmos. Electricity.* Norman, OK, 15pp.

Boggs, L. D., N. Liu, M. Peterson, S. Lazarus, M. Splitt, F. Lucena, A. Nag, and H. Rassoul, 2019: First observations of gigantic jets from geostationary orbit. *Geophys. Res. Lett.*, **46**. https://doi.org/10.1029/2019GL082278

Carey, L. D., M. J. Murphy, T. L. McCormick, and N. W. S. Demetriades, 2005: Lightning location relative to storm structure in a leading-line, trailing-stratiform mesoscale convective system. *J. Geophys. Res.*, **110,** D03105

Christian, H. J., R. J. Blakeslee, S. J. Goodman, and D. M. Mach (Eds.), 2000: Algorithm Theoretical Basis Document (ATBD) for the Lightning Imaging Sensor (LIS), NASA/Marshall Space Flight Center, Alabama. (Available as http://eospso.gsfc.nasa.gov/atbd/listables.html, posted 1 Feb. 2000)

Christian, H. J., et al., Global frequency and distribution of lightning as observed from space by the Optical Transient Detector, *J. Geophys. Res.*, 108(D1), 4005, doi:10.1029/2002JD002347, 2003.

Ely, B. L., R. E. Orville, D. C. Lawrence, and C. L. Hodapp, 2008: Evolution of the total lightning structure in a leading-line, trailing-stratiform mesoscale convective system over Houston, Texas. *J. Gephys. Res*., **113,** doi:10.1029/2007JD008445

Goodman, S. J., D. Mach, W. J. Koshak, and R. J. Blakeslee, 2010: GLM Lightning Cluster-Filter Algorithm (LCFA) Algorithm Theoretical Basis Document (ATBD). NOAA NESDIS Center for Satellite

Applications and Research. (Available as https://www.goes-r.gov/products/ATBDs/baseline/Lightning_v2.0_no_color.pdf, posted 24 Sept. 2010)

Goodman, S. J., R. J. Blakeslee, W. J. Koshak, D. Mach, J. Bailey, D. Buechler, L. Carey, C. Schultz, M. Bateman, E. McCaul Jr., and G. Stano, 2013: The GOES-R geostationary lightning mapper (GLM). *J. Atmos. Res.*, **125-126**, 34-49

Holden, D. N., C. P. Munson, and J. C. Devenport, 1995: Satellite observations of transionospheric pulse pairs, Geophys. Res. Lett., **22**, 889–892

Jacobson, A. R., S. O. Knox, R., Franz, and D. C. Enemark, 1999: FORTE observations of lightning radio-frequency signatures: Capabilities and basic results. *Radio Sci.*, **34** (2), 337– 354, doi:10.1029/1998RS900043

Jacobson, A. R., K. L. Cummins, M. Carter, P. Klingner, D. Roussel-Dupré, and S. O. Knox, 2000: FORTE radio-frequency observations of lightning strokes detected by the National Lightning Detection Network. *J. Geophys. Res.*, **105** (D12), 15653– 15662, doi:10.1029/2000JD900103

Koshak, W. J., R. J. Solakiewicz, D. D. Phanord, and R. J. Blakeslee, 1994: Diffusion model for lightning radiative transfer. *J. Geophys. Res.*, **99**(D7), 14361– 14371, doi:10.1029/94JD00022

Koshak, W. J., 2010: Optical characteristics of OTD flashes and the implications for flash-type discrimination. *J. Atmos. Oceanic. Technol.*, **27,** 1,822 – 1,838

Lang, T. J., S. A. Rutledge, and K. C. Wiens, 2004: Origins of positive cloud-to-ground lightning in the stratiform region of a mesoscale convective system. *Geophys. Res. Lett.*, **31,** doi: 10.1029/2004GL019823

Lang, T., S. Pédeboy, W. Rison, R. Cerveny, J. Montanyà, S. Chauzy, D. MacGorman, R. Holle, E. Ávila, Y. Zhang, G. Carbin, E. Mansell, Y. Kuleshov, T. Peterson, M. Brunet, F. Driouech, and D. Krahenbuhl, 2017: WMO World Record Lightning Extremes: Longest Reported Flash Distance and Longest Reported Flash Duration. *Bull. Amer. Meteor. Soc.* **98**, 1153–1168, https://doi.org/10.1175/BAMS-D-16-0061.1

Lang, T., and S. A. Rutledge, 2008: Kinematic, microphysical, and electrical aspects of an asymmetric bow echo mesoscale convective system observed during STEPS. *J. Geophys. Res.*, **113,** doi: 10.1029/2006JD007709

Light, T. E., D. M. Suszcynsky, M. W. Kirkland, and A. R. Jacobson, 2001a: Simulations of lightning optical waveforms as seen through clouds by satellites. *J. Geophys. Res.*, **106**, D15, 17103–17114, doi: 10.1029/2001JD900051

619 Light, T. E., D. M. Suszcynsky, and A. R. Jacobson, 2001b: Coincident radio frequency and optical emissions from
620 lightning, observed with the FORTE satellite. J. Geophys. Res., 106(D22), 28223– 28231,
621 doi:10.1029/2001JD000727
622 Lojou, J.-Y., K. L. Cummins, 2004: On the representation of two- and three-dimensional total lightning information.
623 In Preprints, Conference on Meteorological Applications of Lightning Data (pp. Paper 2.4, AMS Annual
624 Meeting, San Diego, CA, USA)
625 Marshall, T. C., and W. D. Rust, 1993: Two types of vertical electrical structures in stratiform precipitation regions
626 of mesoscale convective systems. *Bull. Amer. Meteor. Soc.*, **74,** 2159-2170
627 Marshall, T. C., M. Stolzenburg, P. R. Krehbiel, N. R. Lund, and C. R. Maggio, 2009. Electrical evolution during
628 the decay stage of New Mexico thunderstorms, *J. Geophys. Res.*, **114**, D02209, doi:
629 10.1029/2008JD010637
630 Mazur, V., X.-M. Shao, and P. R. Krehbiel, 1998: "Spider" lightning in intracloud and positive cloud-to-ground
631 flashes. *J. Geophys. Res.*, **103** (D16), 19811– 19822, doi:10.1029/98JD02003
632 Peterson, M., 2020, CIERRA-FORTE Flash Cluster Data, https://doi.org/10.7910/DVN/63FWWU, Harvard
633 Dataverse, DRAFT VERSION
634 Peterson, M. J. and C. Liu, 2011: Global statistics of lightning in anvil and stratiform regions over the tropics and
635 subtropics observed by TRMM, *J. Geophys. Res.*, **116**, D23, doi: 10.1029/2011JD015908
636 Peterson, M. J. and C. Liu, 2013: Characteristics of lightning flashes with exceptional illuminated areas, durations,
637 and optical powers and surrounding storm properties in the tropics and inner subtropics, *J. Geophys. Res.*,
638 **118**, 11,727-11,740, doi: 10.1002/jgrd.50715
639 Peterson, M. J., W. Deierling, C. Liu, D. Mach, C. Kalb, 2017a: The properties of optical lightning flashes and the
640 clouds they illuminate. *J. Geophys. Res. Atmos*., **122**, 423–442, doi:10.1002/2016JD025312
641 Peterson, M. J., S. Rudlosky, and W. Deierling, 2017b: The evolution and structure of extreme optical lightning
642 flashes. *J. Geophys. Res. Atmos*., **122**, doi: 10.1002/2017JD026855
643 Peterson, M., S. Rudlosky, and W. Deierling, 2018: Mapping the Lateral Development of Lightning Flashes from
644 Orbit. *J. Geophys. Res. Atmos.*, **123**, 9674– 9687. https://doi.org/10.1029/2018JD028583
645 Peterson, M., S. Rudlosky, 2019: The time evolution of optical lightning flashes. *J. Gephys. Res.*, **124**, 333– 349.
646 https://doi.org/10.1029/2018JD028741

Peterson, M., T. E. L. Light, and X.-M. Shao, 2020a: Combined Optical and Radio-Frequency Perspectives on Hybrid Cloud-to-Ground Lightning Observed by the FORTE Satellite, this issue (submitted as companion paper)

Prueitt, M. L., 1963: The excitation temperature of lightning. *J. Geophys. Res.*, **68** (3), 803– 811, doi:10.1029/JZ068i003p00803

Rison, W., R.J. Thomas, P.R. Krehbiel, T. Hamlin, and J. Harlin, 1999: A GPS-based three-dimensional lightning mapping system: initial observations in central New Mexico. *Geophys. Res. Lett*., **26**, 23, 3573-3576

Rutledge, S. A., and D. R. MacGorman, 1988: Cloud-to-ground lightning activity in the 10-11 June 1985 mesoscale convective system observed during the Oklahoma-Kansas PRESTORM project. *Mon. Wea. Rev.*, **116**, 1393–1408

SSEC, 2019: Satellite Data Services Inventory. Accessed 7 May 2019, https://qcweb.ssec.wisc.edu/inventory/

Stolzenburg, M., T.C. Marshall, W. D. Rust, and B.F. Smull, 1994: Horizontal distribution of electrical and meteorological conditions across the stratiform region of a mesoscale convective system. *Mon. Wea. Rev.*, **122,** 1777–1797

Suszcynsky, D. M., M. W. Kirkland, A. R., Jacobson, R. C. Franz, S. O. Knox, J. L. L. Guillen, and J. L. Green, 2000: FORTE observations of simultaneous VHF and optical emissions from lightning: Basic phenomenology. *J. Geophys. Res.*, **105** (D2), 2191– 2201, doi:10.1029/1999JD900993

Suszcynsky, D. M., T. E. Light, S., Davis, J. L., Green, J. L. L. Guillen, and W. Myre, 2001: Coordinated observations of optical lightning from space using the FORTE photodiode detector and CCD imager. *J. Geophys. Res.*, **106** (D16), 17897– 17906, doi:10.1029/2001JD900199

Thomas, R., P.R. Krehbiel, W. Rison, T. Hamlin, D. J. Boccippio, S. J. Goodman, and H. J. Christian, 2000: Comparison of ground-based 3-dimensional lightning mapping observations with satellite-based LIS observations in Oklahoma. *Geophys. Res. Lett.*, **27**, 12, 1,703-1,706.

Thomson, L.W. and E.P. Krider, 1982: The Effects of Clouds on the Light Produced by Lightning. *J. Atmos. Sci.*, **39**, 2051–2065, https://doi.org/10.1175/1520-0469(1982)039<2051:TEOCOT>2.0.CO;2

Tillier, C. E., S. F. Edgington, H. J. Christian, and P. M. Bitzer, 2019: The First Stereo Views of Lightning from Space: Double the GLMs, Double the Fun. *99th American Meteorological Society Annual Meeting*,

674 Phoenix, AZ, Amer. Meteor. Soc., TJ11.1,
675 https://ams.confex.com/ams/2019Annual/webprogram/Paper350902.html
676 Winn, W. P., G. D. Aulich, S. J. Hunyady, K. B. Eack, H. E. Edens, P. R. Krehbiel, W. Rison, and R. G.
677 Sonnenfeld, 2011: Lightning leader stepping, K changes, and other observations near an intracloud flash. *J.*
678 *Geophys. Res.*, **116**, D23115, doi:10.1029/2011JD015998

679
680

681

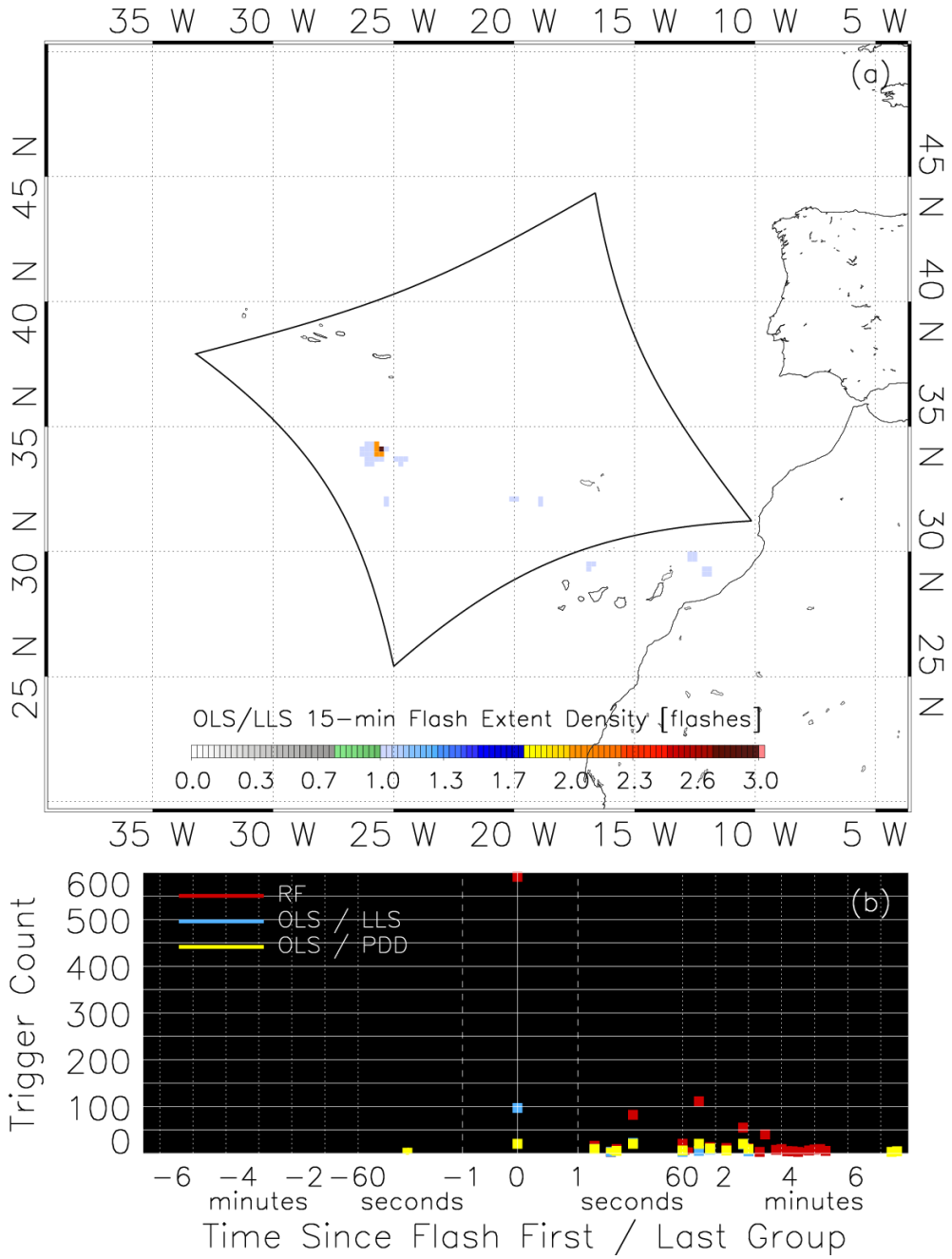

682
683

684 **Figure 1.** FORTE LLS lightning activity near the flash of interest. (a) FED across the LLS FOV and (b) optical and
685 RF trigger rates during the 15-minute window surrounding the flash. Because lightning was infrequent across the
686 FORTE FOV during the flash window, triggers from other flashes are unlikely.

687

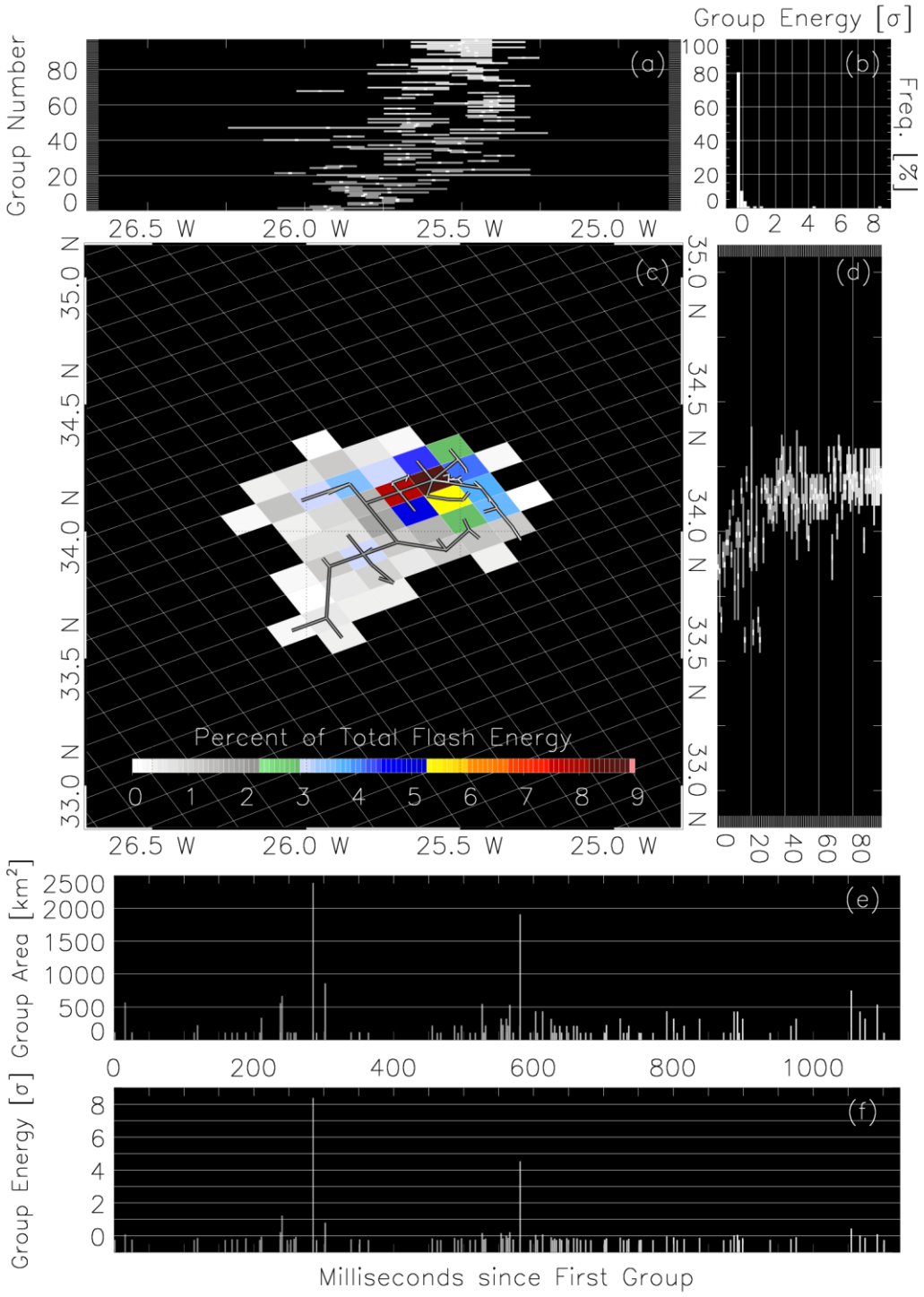

Figure 2. Evolution plot for the LLS flash. (a) group extent by longitude, (b) group energy distribution, (c) plan view of flash energy (color contour) and group extent (line segments), (d) group extent by latitude, (e) timeseries of group area, and (f) timeseries of group energy. Group energies are expressed as a sigma level relative to the average group energy in the flash. The greyscale in all plots represents the group number.

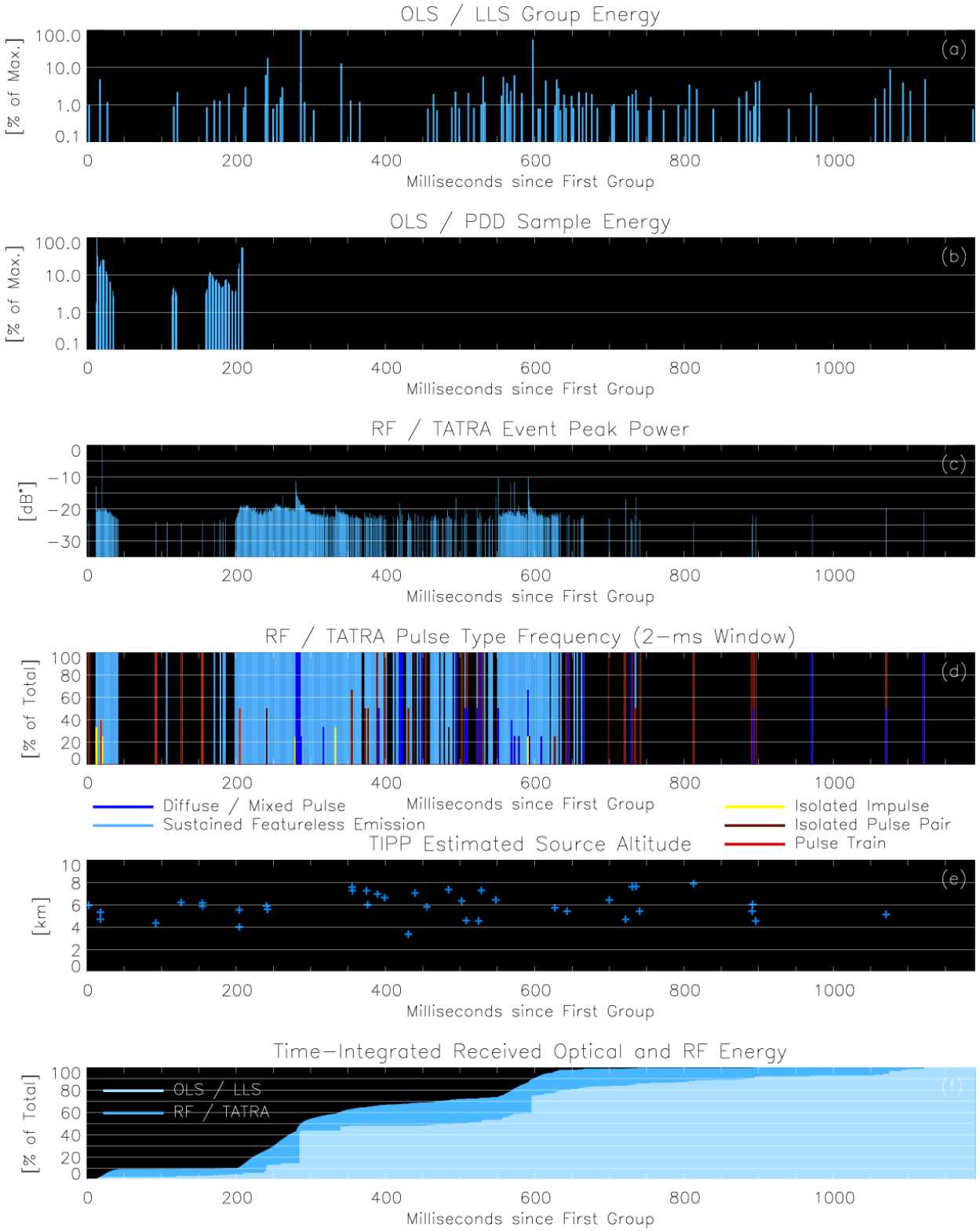

Figure 3. Timeseries showing the combined optical / RF evolution of the flash. (a) LLS and (b) optical energies. (c) TATR event peak RF power. (d) TATR pulse classification shown as the frequency of each pulse type in a 2-ms window. (e) estimated altitude of in-cloud (TIPP) sources. (f) time-integrated optical and RF energies over the flash duration

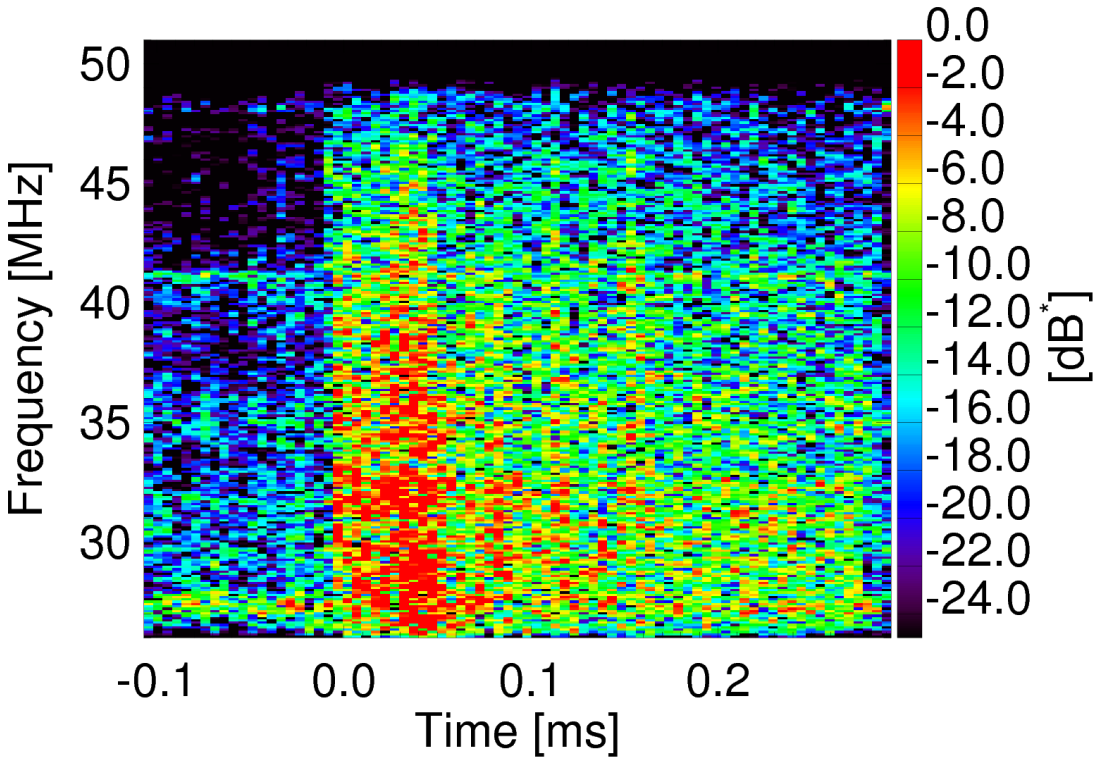

Figure 4. Spectrogram showing normalized RF power over the lowband frequency range as a function of time sensed by TATR during the first +CG event at 14 ms into the LLS flash. The sharp onset and long-duration pulse are common VHF features associated with +CGs.

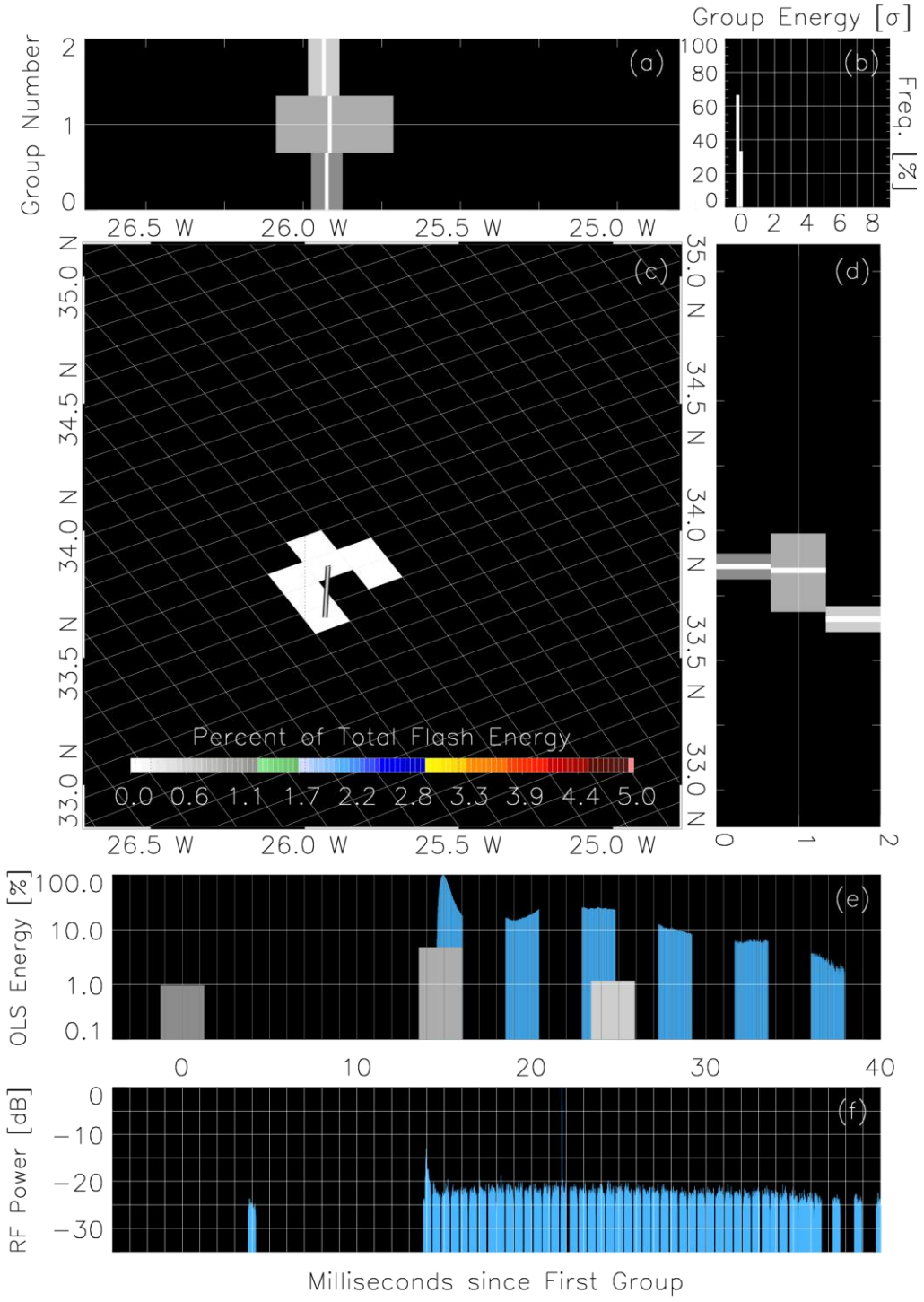

Figure 5. Evolution plot for the first 40 ms of optical triggers in the flash. Identical to Figure 3, but with LLS group area replaced by TATR RF power (f) and PDD data plotted blue in (e)

712

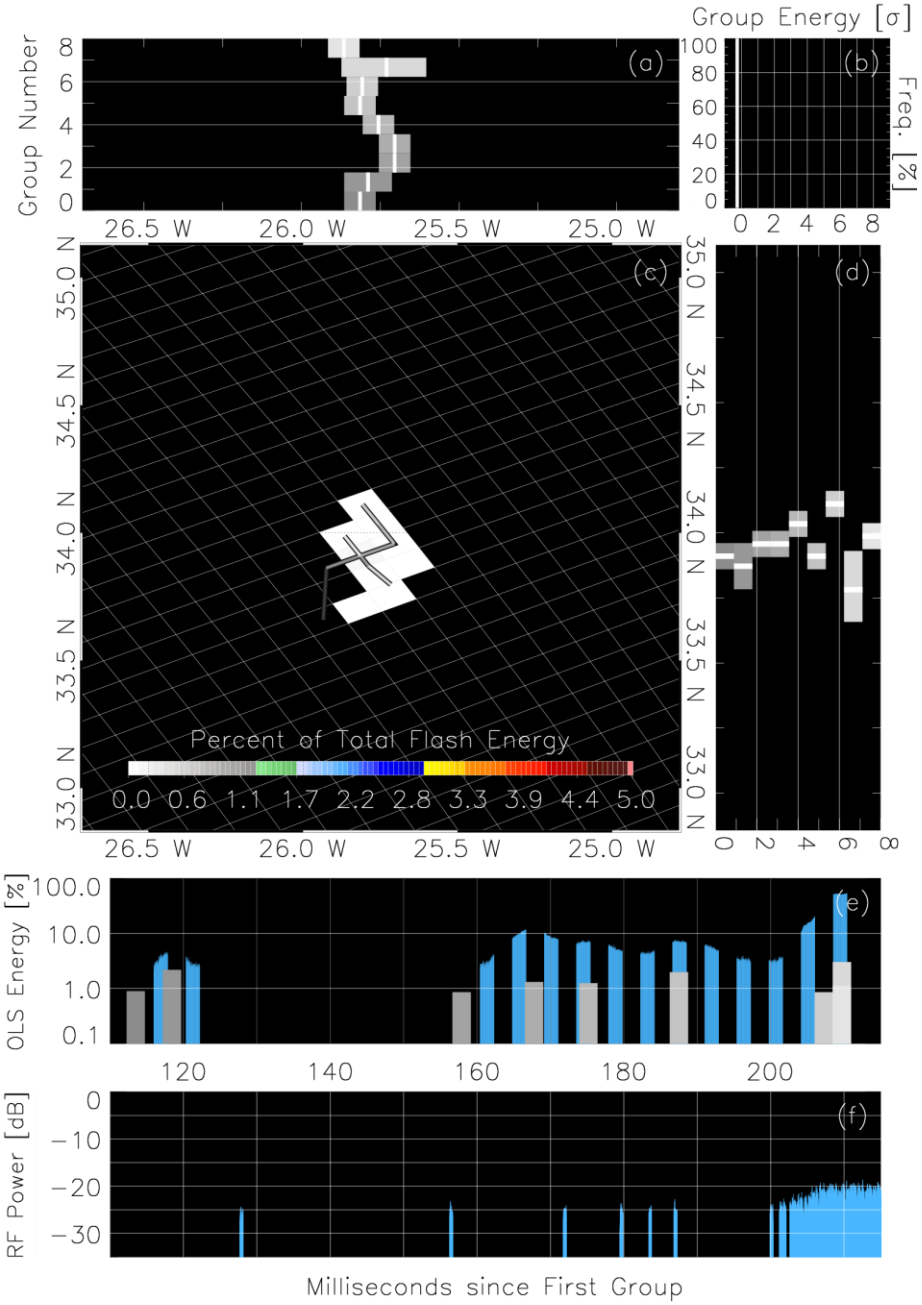

713
714 **Figure 6.** Same as Figure 5, but for the period 110 ms – 215 ms that begins the longest period of sustained PDD /
715 TATR triggering
716

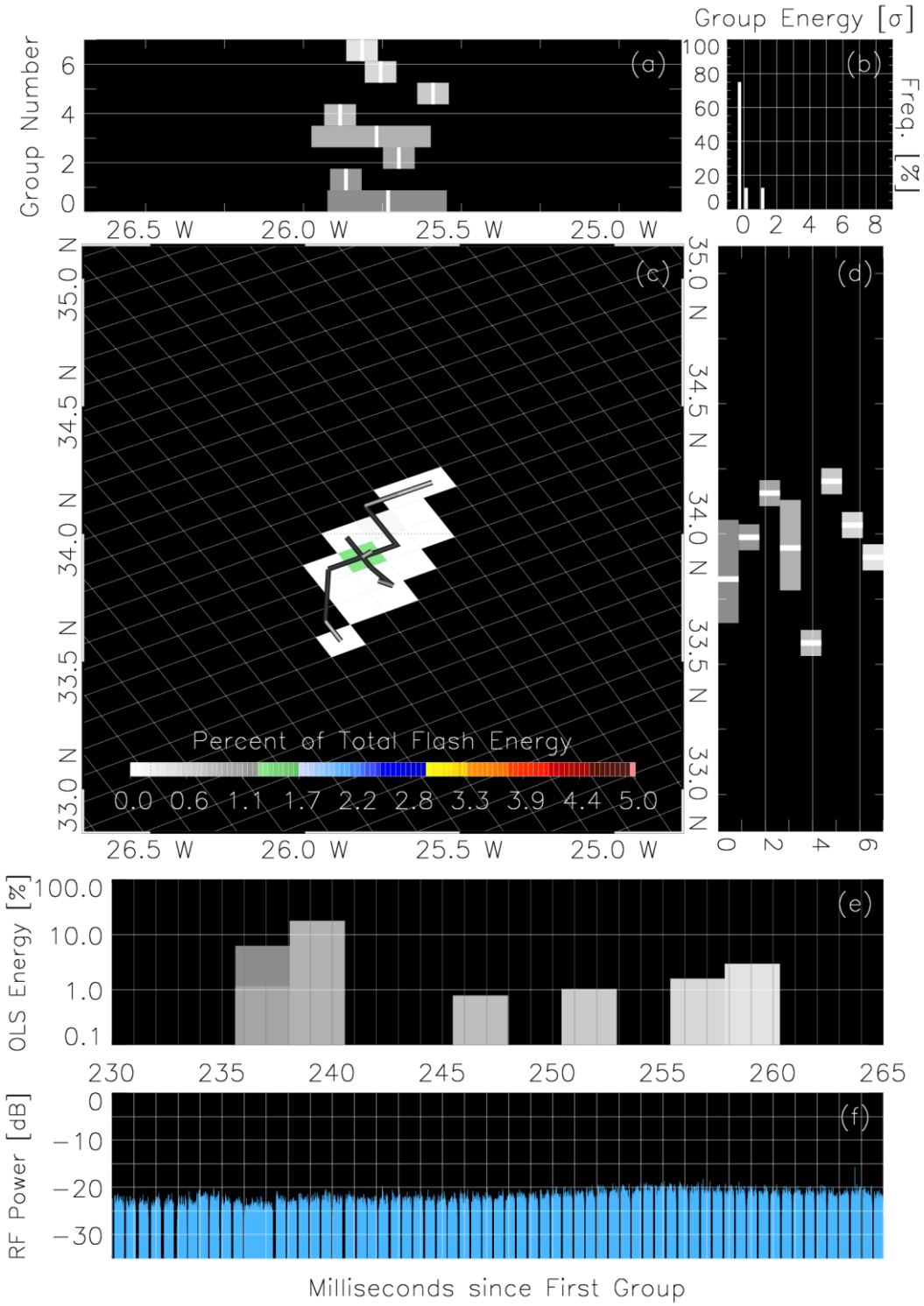

Figure 7. Same as Figure 5, but for the period 230 ms – 265 ms during the initial development phase of the spider flash

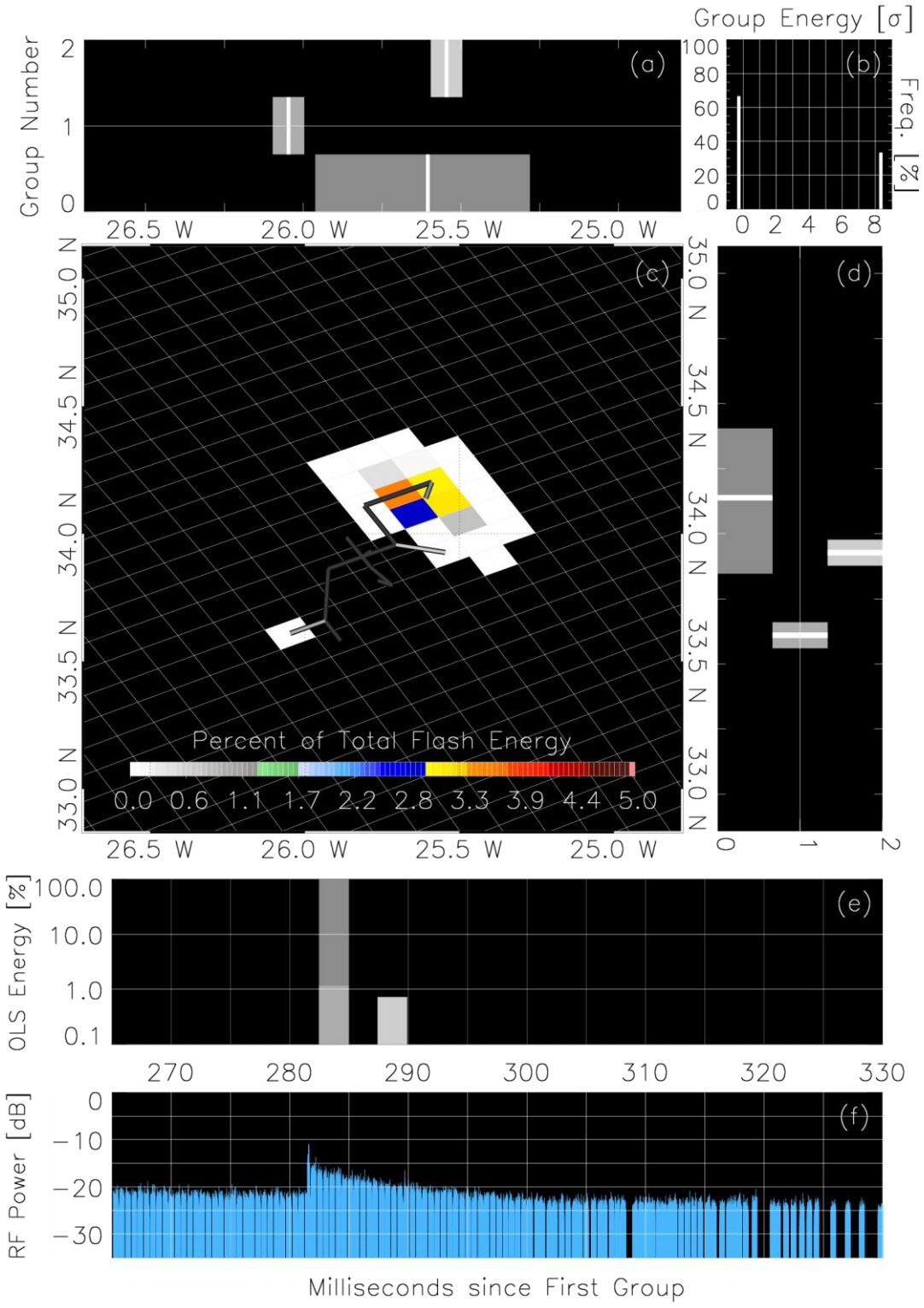

Figure 8. Same as Figure 5, but for the period 265 ms – 330 ms that includes the first possible +CG stroke

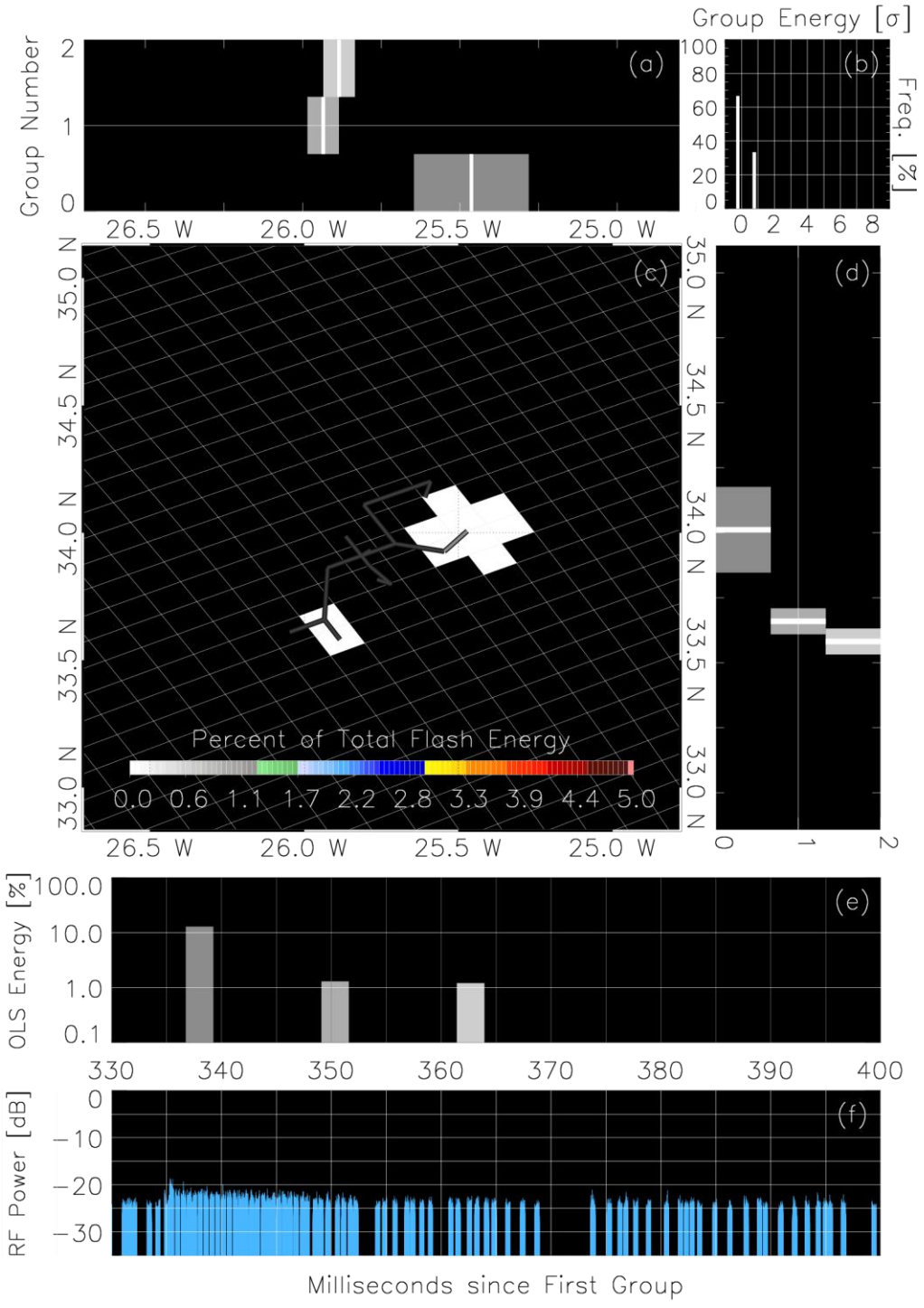

Figure 9. Same as Figure 5, but for the period 330 ms – 400 ms that shows a possible (questionable) second +CG stroke in a different location than Figure 8

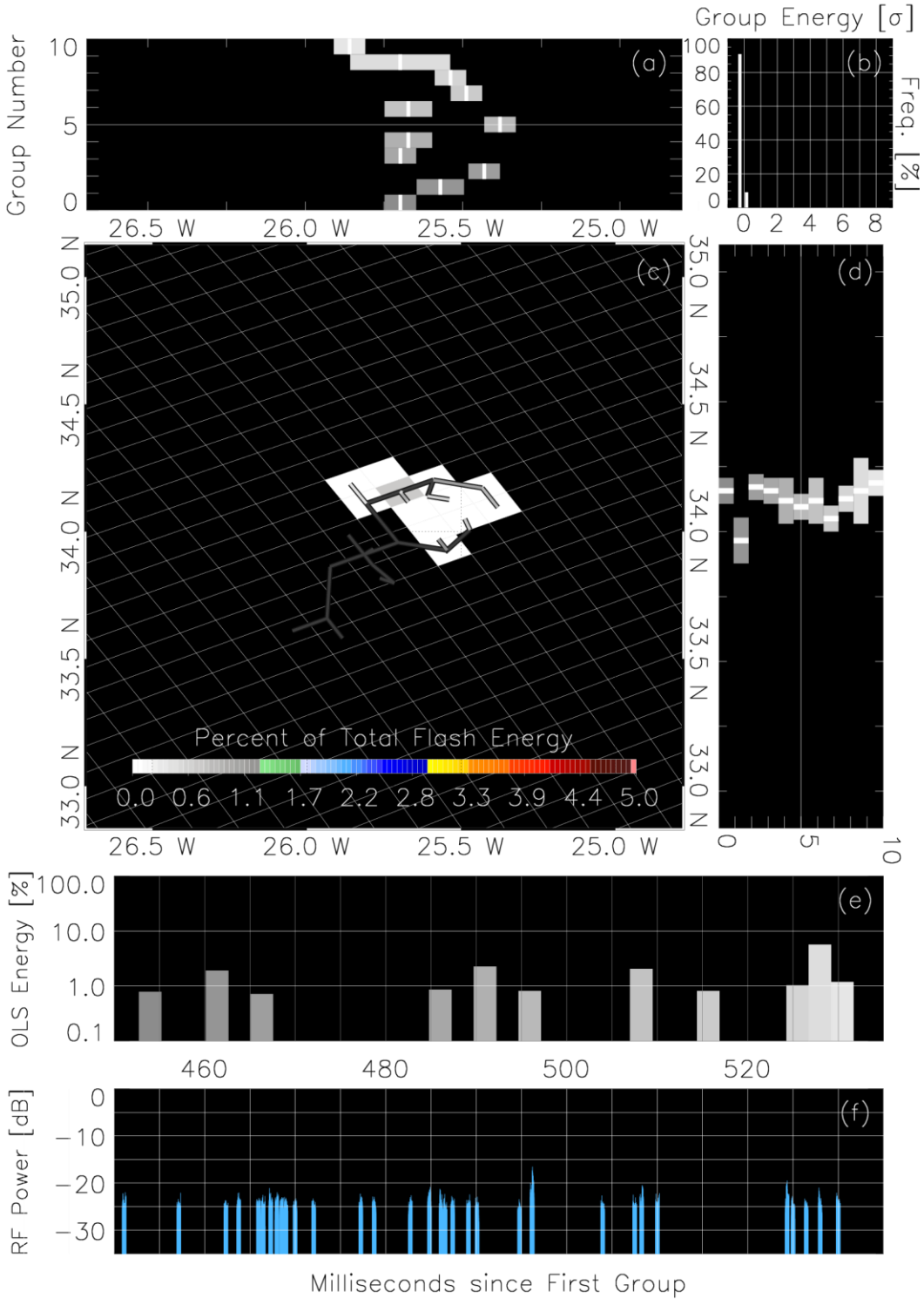

Figure 10. Same as Figure 5, but for the period 450 ms – 535 ms showing additional lateral development ending with the start of a new main branch to the northwest

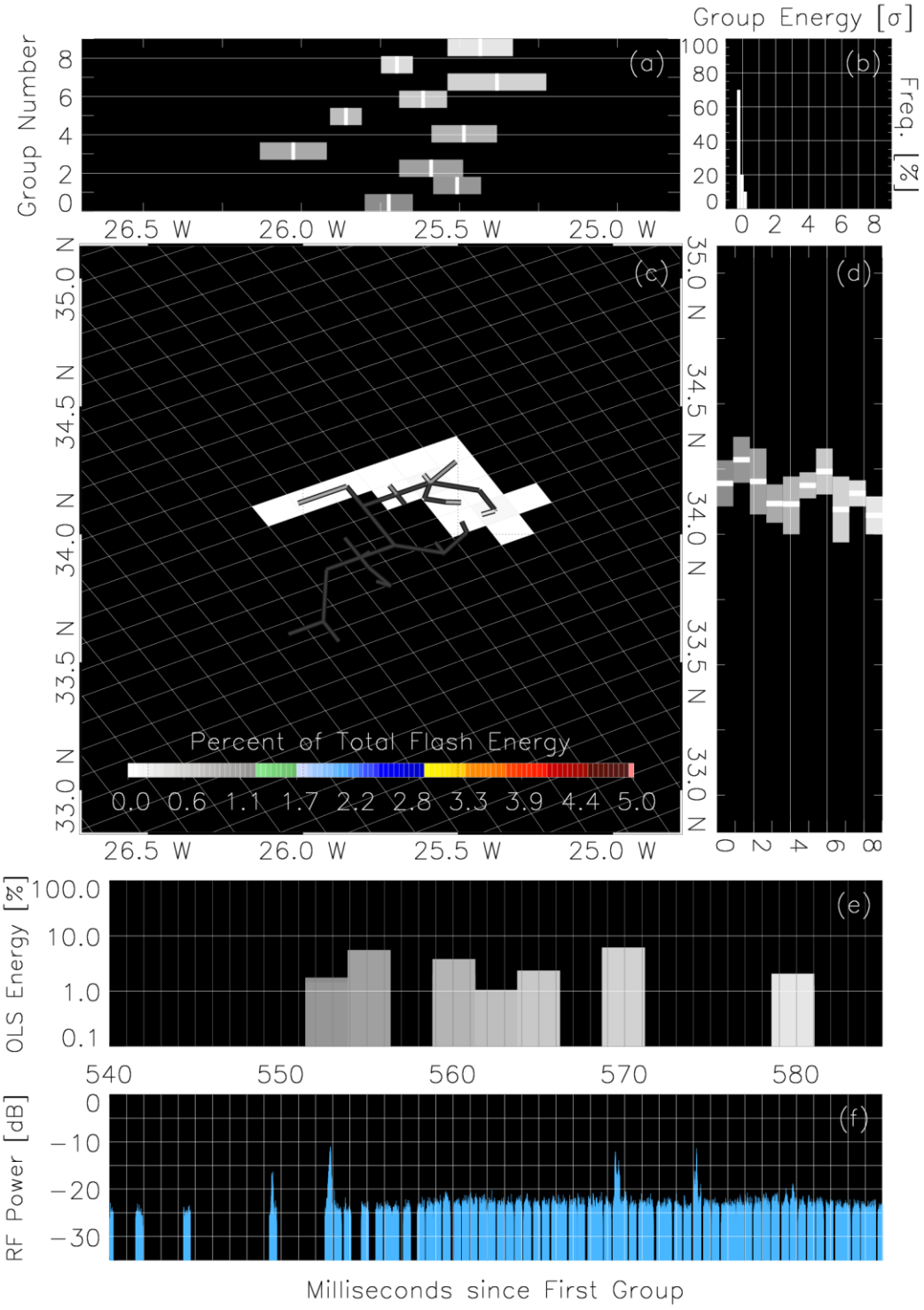

Figure 11. Same as Figure 5, but for the period 540 ms – 585 ms where sustained TATR triggering resumes after a diffuse VHF pulse

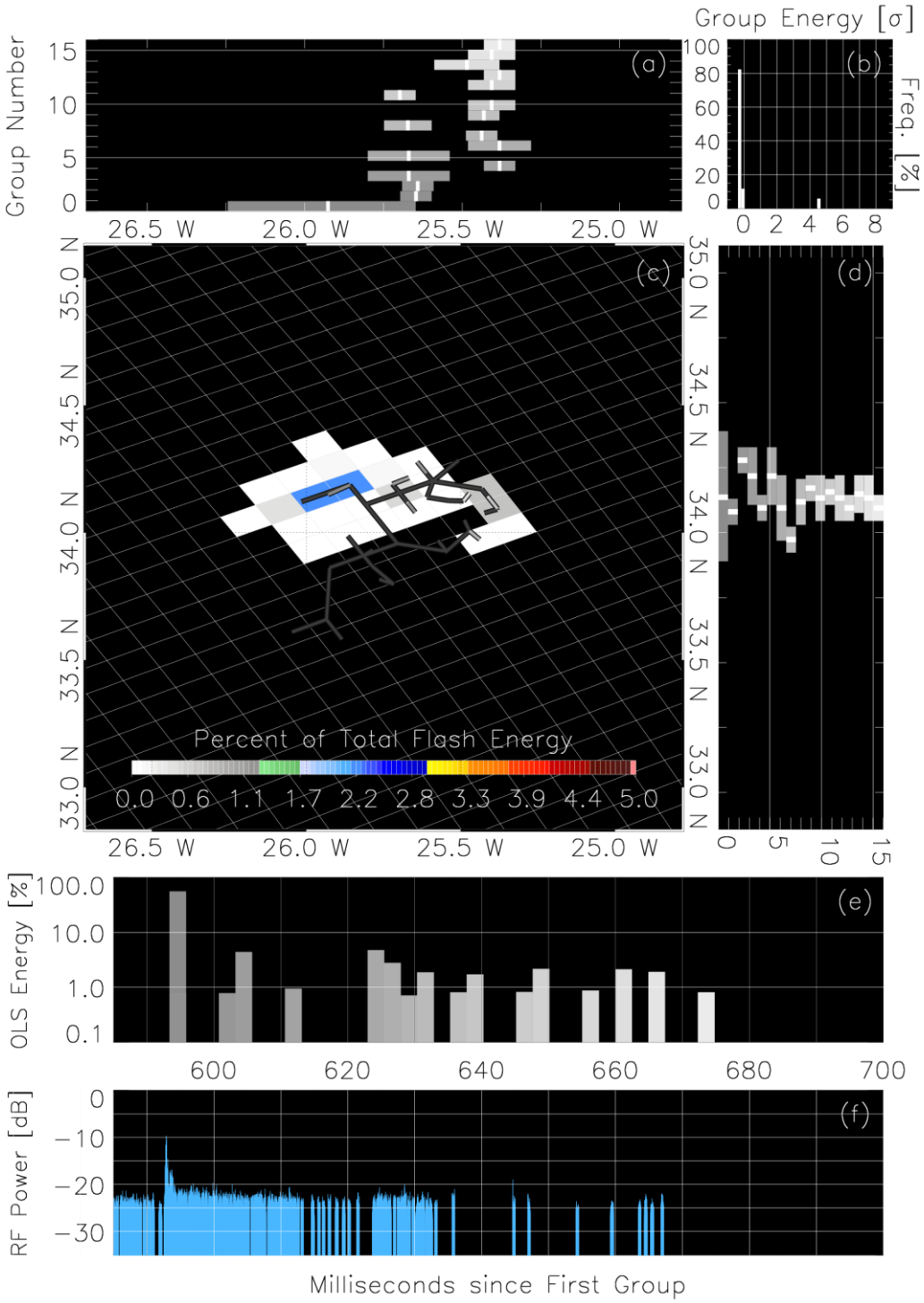

Figure 12. Same as Figure 5, but for the period 585 ms – 700 ms showing a possible (questionable) third +CG stroke along the new northwest branch

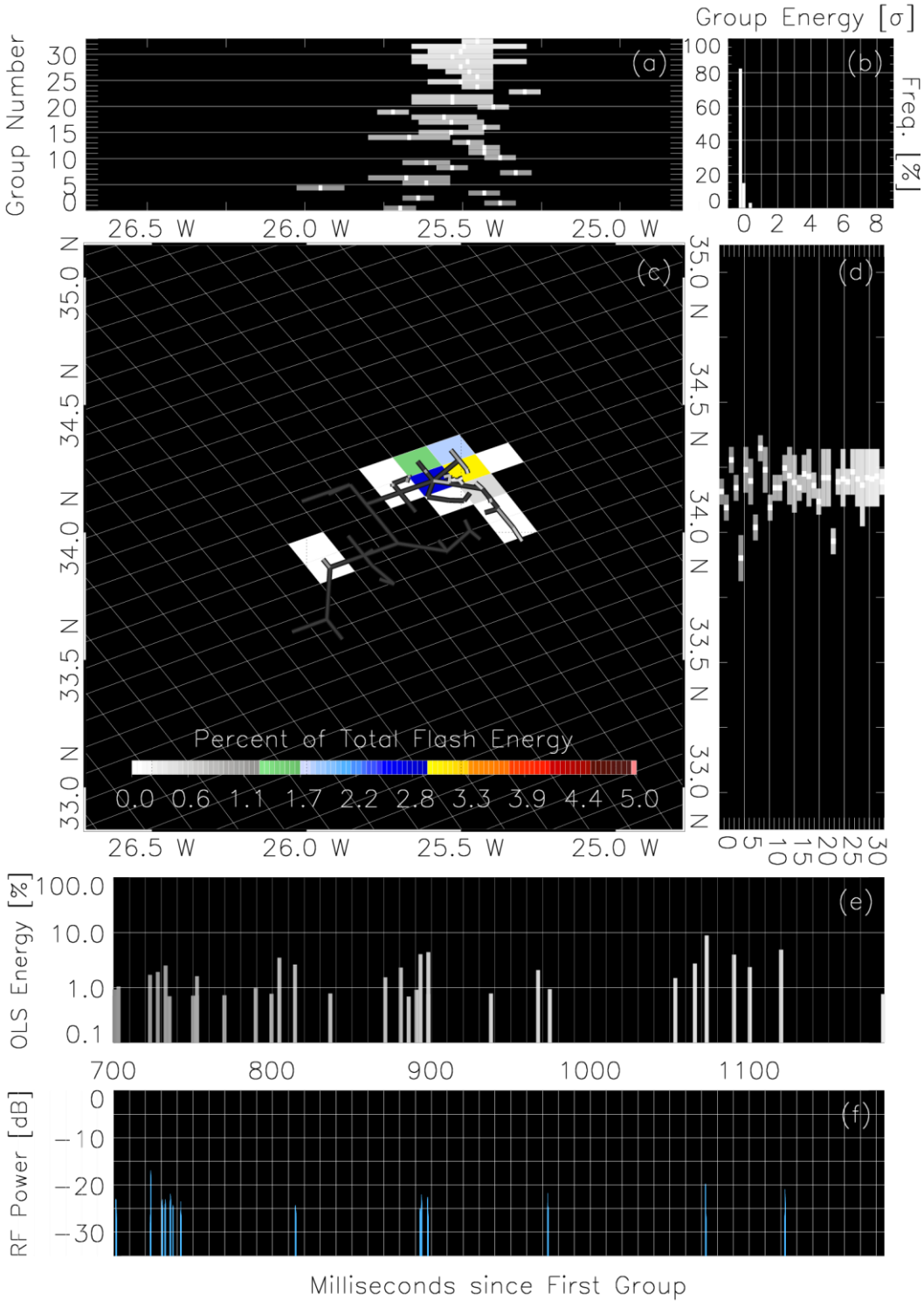

Figure 13. Same as Figure 5, but for the period 700 ms – 1180 ms that documents the final LLS / TATR pulses after the sustained VHF emission has ceased

Figure 1.

35 W 30 W 25 W 20 W 15 W 10 W 5 W

45 N 40 N 35 N 30 N 25 N

(a)

OLS/LLS 15-min Flash Extent Density [flashes]

0.0 0.3 0.7 1.0 1.3 1.7 2.0 2.3 2.6 3.0

35 W 30 W 25 W 20 W 15 W 10 W 5 W

(b)

RF

OLS / LLS

OLS / PDD

Trigger Count

600 500 400 300 200 100 0

−6 −4 −2 −60 −1 0 1 60 2 4 6

minutes seconds seconds minutes

Time Since Flash First / Last Group

Figure 2.

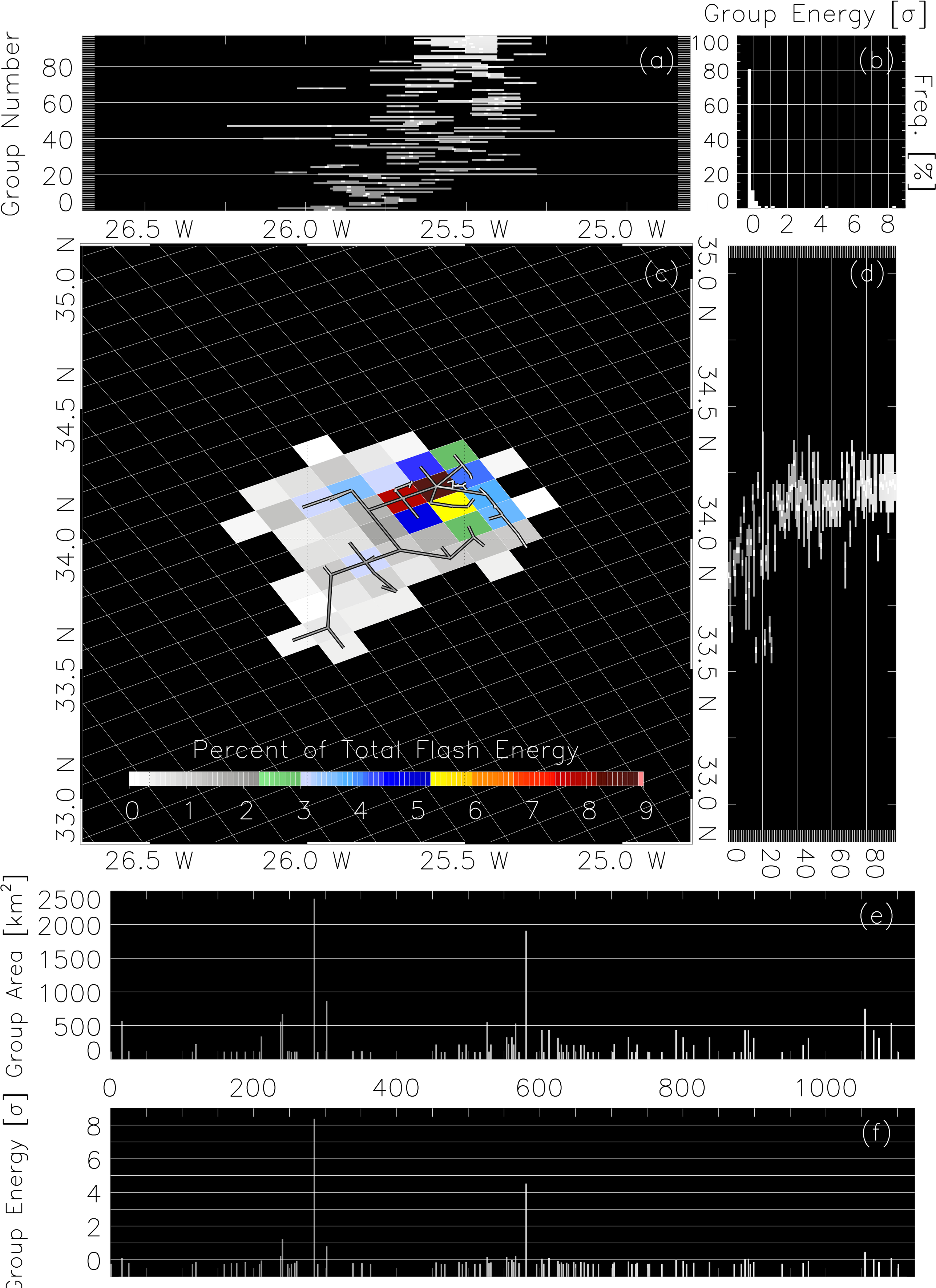
Group Number
(a)
Group Energy [σ]
(b)
Freq. [%]
26.5 W
26.0 W
25.5 W
25.0 W
35.0 N
34.5 N
34.0 N
33.5 N
33.0 N
(c)
Percent of Total Flash Energy
(d)
Group Area [km²]
(e)
Group Energy [σ]
(f)
Milliseconds since First Group

Figure 3.

OLS / LLS Group Energy

[% of Max.]

100.0
10.0
1.0
0.1

(a)

0 200 400 600 800 1000

Milliseconds since First Group

OLS / PDD Sample Energy

[% of Max.]

100.0
10.0
1.0
0.1

(b)

0 200 400 600 800 1000

Milliseconds since First Group

RF / TATRA Event Peak Power

[dB*]

0
−10
−20
−30

(c)

0 200 400 600 800 1000

Milliseconds since First Group

RF / TATRA Pulse Type Frequency (2−ms Window)

[% of Total]

100
80
60
40
20
0

(d)

0 200 400 600 800 1000

Milliseconds since First Group

Diffuse / Mixed Pulse
Sustained Featureless Emission
Isolated Impulse
Isolated Pulse Pair
Pulse Train

TIPP Estimated Source Altitude

[km]

10
8
6
4
2
0

(e)

0 200 400 600 800 1000

Milliseconds since First Group

Time−Integrated Received Optical and RF Energy

[% of Total]

100
80
60
40
20
0

OLS / LLS
RF / TATRA

(f)

0 200 400 600 800 1000

Milliseconds since First Group

Figure 4.

Frequency [MHz]

50
45
40
35
30

-0.1
0.0
0.1
0.2

Time [ms]

0.0
-2.0
-4.0
-6.0
-8.0
-10.0
-12.0
-14.0
-16.0
-18.0
-20.0
-22.0
-24.0

[dB]

Figure 5.

Group Number

Group Energy [σ]

(a)

(b)

Freq. [%]

(c)

(d)

Percent of Total Flash Energy

(e)

OLS Energy [%]

(f)

RF Power [dB]

Milliseconds since First Group

Figure 6.

Group Number

Group Energy [σ]

(a)

(b)

Freq. [%]

(c)

(d)

Percent of Total Flash Energy

0.0 0.6 1.1 1.7 2.2 2.8 3.3 3.9 4.4 5.0

OLS Energy [%]

(e)

RF Power [dB]

(f)

Milliseconds since First Group

Figure 7.

(a)

Group Number

0 2 4 6

26.5 W 26.0 W 25.5 W 25.0 W

(b)

Group Energy [σ]

Freq. [%]

100 80 60 40 20 0

0 2 4 6 8

(c)

35.0 N 34.5 N 34.0 N 33.5 N 33.0 N

Percent of Total Flash Energy

0.0 0.6 1.1 1.7 2.2 2.8 3.3 3.9 4.4 5.0

26.5 W 26.0 W 25.5 W 25.0 W

(d)

35.0 N 34.5 N 34.0 N 33.5 N 33.0 N

0 2 4 6

(e)

OLS Energy [%]

100.0 10.0 1.0 0.1

230 235 240 245 250 255 260 265

(f)

RF Power [dB]

0 −10 −20 −30

Milliseconds since First Group

Figure 8.

Group Number
2
1
0
(a)
26.5 W
26.0 W
25.5 W
25.0 W
Group Energy [σ]
100
80
60
40
20
0
(b)
Freq. [%]
0
2
4
6
8
35.0 N
34.5 N
34.0 N
33.5 N
33.0 N
(c)
Percent of Total Flash Energy
0.0 0.6 1.1 1.7 2.2 2.8 3.3 3.9 4.4 5.0
(d)
OLS Energy [%]
100.0
10.0
1.0
0.1
(e)
270
280
290
300
310
320
330
RF Power [dB]
0
−10
−20
−30
(f)
Milliseconds since First Group

Figure 9.

Group Number

(a)

Group Energy [σ]

(b)

Freq. [%]

26.5 W 26.0 W 25.5 W 25.0 W

35.0 N 34.5 N 34.0 N 33.5 N 33.0 N

(c)

Percent of Total Flash Energy

(d)

OLS Energy [%]

(e)

RF Power [dB]

(f)

Milliseconds since First Group

Figure 10.

Group Number
10
5
0
(a)
Group Energy [σ]
100
80
60
40
20
0
(b)
Freq. [%]
0
2
4
6
8
26.5 W
26.0 W
25.5 W
25.0 W
35.0 N
34.5 N
34.0 N
33.5 N
33.0 N
(c)
Percent of Total Flash Energy
0.0 0.6 1.1 1.7 2.2 2.8 3.3 3.9 4.4 5.0
(d)
0
5
10
OLS Energy [%]
100.0
10.0
1.0
0.1
(e)
460
480
500
520
RF Power [dB]
0
−10
−20
−30
(f)
Milliseconds since First Group

Figure 11.

Group Number

(a)

Group Energy [σ]

(b)

Freq. [%]

26.5 W 26.0 W 25.5 W 25.0 W

35.0 N 34.5 N 34.0 N 33.5 N 33.0 N

(c)

Percent of Total Flash Energy

0.0 0.6 1.1 1.7 2.2 2.8 3.3 3.9 4.4 5.0

(d)

OLS Energy [%]

(e)

RF Power [dB]

(f)

Milliseconds since First Group

Figure 12.

Group Number

15
10
5
0

(a)

Group Energy [σ]

100
80
60
40
20
0

(b)

Freq. [%]

0 2 4 6 8

26.5 W 26.0 W 25.5 W 25.0 W

35.0 N
34.5 N
34.0 N
33.5 N
33.0 N

(c)

Percent of Total Flash Energy

0.0 0.6 1.1 1.7 2.2 2.8 3.3 3.9 4.4 5.0

26.5 W 26.0 W 25.5 W 25.0 W

35.0 N
34.5 N
34.0 N
33.5 N
33.0 N

(d)

0 5 10 15

OLS Energy [%]

100.0
10.0
1.0
0.1

(e)

600 620 640 660 680 700

RF Power [dB]

0
−10
−20
−30

(f)

Milliseconds since First Group

Figure 13.

Group Number

Group Energy [σ]

(a)

(b)

Freq. [%]

(c)

(d)

Percent of Total Flash Energy

OLS Energy [%]

(e)

RF Power [dB]

(f)

Milliseconds since First Group